

NAVAL POSTGRADUATE SCHOOL MONTEREY, CALIFORNIA



THESIS

ANALYSIS OF HYPERSPECTRAL DATA USING POLARIMETRIC CHARACTERISTICS

by

David Scott Petri

December, 1996

Thesis Advisor:
Co-Advisor:

D. D. Cleary
R. C. Olsen

Approved for public release; distribution is unlimited.

19970801 049

DTIC QUALITY INSPECTED 1

REPORT DOCUMENTATION PAGE			Form Approved OMB No. 0704-0188	
Public reporting burden for this collection of information is estimated to average 1 hour per response, including the time for reviewing instruction, searching existing data sources, gathering and maintaining the data needed, and completing and reviewing the collection of information. Send comments regarding this burden estimate or any other aspect of this collection of information, including suggestions for reducing this burden, to Washington Headquarters Services, Directorate for Information Operations and Reports, 1215 Jefferson Davis Highway, Suite 1204, Arlington, VA 22202-4302, and to the Office of Management and Budget, Paperwork Reduction Project (0704-0188) Washington DC 20503.				
1. AGENCY USE ONLY (Leave blank)	2. REPORT DATE December 1996.	3. REPORT TYPE AND DATES COVERED Master's Thesis		
4. ANALYSIS OF HYPERSPECTRAL DATA USING POLARIMETRIC CHARACTERISTICS		5. FUNDING NUMBERS		
6. AUTHOR(S) David Scott Petri				
7. PERFORMING ORGANIZATION NAME(S) AND ADDRESS(ES) Naval Postgraduate School Monterey CA 93943-5000		8. PERFORMING ORGANIZATION REPORT NUMBER		
9. SPONSORING/MONITORING AGENCY NAME(S) AND ADDRESS(ES)		10. SPONSORING/MONITORING AGENCY REPORT NUMBER		
11. SUPPLEMENTARY NOTES The views expressed in this thesis are those of the author and do not reflect the official policy or position of the Department of Defense or the U.S. Government.				
12a. DISTRIBUTION/AVAILABILITY STATEMENT Approved for public release; distribution is unlimited.		12b. DISTRIBUTION CODE		
13. ABSTRACT (maximum 200 words) The utility of polarimetric reflectance characteristics of targets and background surfaces in the analysis of hyperspectral imagery data is investigated. A technique is proposed for filtering a data hypercube of an imaged scene to select targets for subsequent analysis using standard hyperspectral signature matching techniques, thereby reducing image analysis time. An experimental study to measure polarization characteristics of reflected light from various surfaces in order to determine wavelengths for maximum and minimum intensity differences between polarized reflectance values is proposed. A second study is outlined for collection of simulated hyperspectral imagery that would attempt to validate the proposed filtering technique. A research of past studies indicate that useful polarization signature components are present for many targets and target materials. Additionally, backgrounds composed of grass, trees, dirt and clouds generate very little polarized components making detection of targets using polarization signatures feasible.				
14. SUBJECT TERMS: Hyperspectral, Polarimetric, Remote Sensing, Imagery, Target Detection, Support to Military Operations			15. NUMBER OF PAGES 88	
			16. PRICE CODE	
17. SECURITY CLASSIFICATION OF REPORT Unclassified	18. SECURITY CLASSIFICATION OF THIS PAGE Unclassified	19. SECURITY CLASSIFICATION OF ABSTRACT Unclassified	20. LIMITATION OF ABSTRACT UL	

Approved for public release; distribution is unlimited.

**ANALYSIS OF HYPERSPECTRAL DATA USING POLARIMETRIC
CHARACTERISTICS**

David Scott Petri
Commander, United States Navy
B.S., United States Naval Academy, 1980

Submitted in partial fulfillment
of the requirements for the degree of

**MASTER OF SCIENCE IN SYSTEMS TECHNOLOGY
(SPACE SYSTEMS OPERATIONS)**

from the

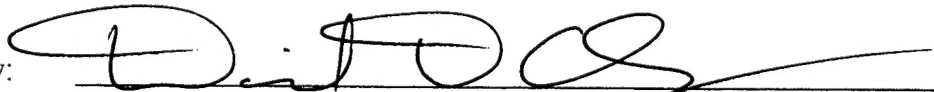
**NAVAL POSTGRADUATE SCHOOL
December 1996**

Author:



David Scott Petri

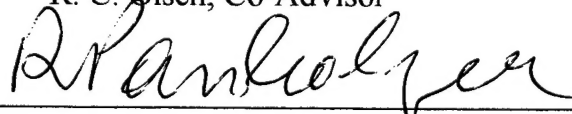
Approved by:



D. D. Cleary, Thesis Advisor



R. C. Olsen, Co-Advisor



Rudy Panholzer, Chairman
Space Systems Academic Group

ABSTRACT

The utility of polarimetric reflectance characteristics of targets and background surfaces in the analysis of hyperspectral imagery data is investigated. A technique is proposed for filtering a data hypercube of an imaged scene to select targets for subsequent analysis using standard hyperspectral signature matching techniques, thereby reducing image analysis time. An experimental study to measure polarization characteristics of reflected light from various surfaces in order to determine wavelengths for maximum and minimum intensity differences between polarized reflectance values is proposed. A second study is outlined for collection of simulated hyperspectral imagery that would attempt to validate the proposed filtering technique. A research of past studies indicate that useful polarization signature components are present for many targets and target materials. Additionally, backgrounds composed of grass, trees, dirt and clouds generate very little polarized components making detection of targets using polarization signatures feasible.

TABLE OF CONTENTS

I.	INTRODUCTION	1
A.	BACKGROUND	1
B.	THESIS OBJECTIVES	2
C.	THESIS OUTLINE	3
II.	REMOTE SENSING	5
A.	FUNDAMENTALS OF REMOTE SENSING	5
1.	Reflective and Emissive Bands	6
2.	Interaction of Light with Objects	7
3.	Sources of Spectral Variation	8
4.	Spectral Reflectance	11
5.	Reflection of Light	15
B.	SPECTRAL IMAGING	16
1.	Hyperspectral Imaging	18
2.	Basic Hyperspectral Imager Designs	20
C.	MILITARY AND NATIONAL SECURITY INVOLVEMENT IN HYPERSPSPECTRAL SENSORS	23
1.	Description of Selected DoD Related Sensor Programs	23
a.	HYMSMO Program	23
b.	HRIS Program	25
c.	SEBASS Program	25
d.	Warfighter-1 Program	25
2.	Tactical Employment Challenges of the Warfighter-1	27
III.	POLARIZATION	29
A.	POLARIZATION STATE OF AN ELECTROMAGNETIC WAVE ...	29
1.	Linear Polarization	31
2.	Circular Polarization	33

3.	Elliptical Polarization	34
B.	POLARIZATION STATE OF LIGHT	35
C.	SOURCES OF POLARIZATION	38
1.	Fresnel Equations	39
2.	Reflection from a Non-conducting Material	43
3.	Reflection from a Conducting Material	47
4.	Selective Absorption	50
D.	REVIEW OF POLARIZATION DETECTION STUDIES	51
1.	Polarization Characterization for Target Surfaces	51
2.	Midwave Infrared Polarization	52
3.	Polarimetric Analysis of Hyperspectral Data in the Visible Spectrum	58
IV.	PROPOSED APPLICATION OF POLARIMETRIC DATA TO HYPERSPPECTRAL IMAGERY ANALYSIS	59
A.	DESCRIPTION OF ANALYSIS TECHNIQUE	59
B.	EXPERIMENT DESIGN	64
1.	Spectral Variation of Polarization	64
a.	Instrumentation	64
b.	Data Collection	67
c.	Data Analysis	69
2.	Polarized Hyperspectral Imagery	69
a.	Instrumentation	70
b.	Data Collection	71
c.	Data Analysis	73
V.	SUMMARY AND RECOMMENDATIONS	75
A.	SUMMARY	75
B.	RECOMMENDATIONS	76
	LIST OF REFERENCES	77
	INITIAL DISTRIBUTION LIST	79

I. INTRODUCTION

The Information Age has made a profound change in the way businesses and governments operate. The ability to communicate from anywhere to anyone has enhanced the flow of information across any border and has created an environment which requires faster decision making. The need for timely and accurate information in order to be competitive belongs not only in the realm of international economics and politics, but military operations as well. The decision cycle used by a military commander is driven by the cycle time of his opponent. The commander able to maintain his decision cycle within the enemy's is surer of victory. Knowledge of the battlefield is paramount. New methods which enhance the intelligence collection effort are continually being developed. One such method being developed is the use of a form of remote sensing known as hyperspectral imagery or imaging spectroscopy.

A. BACKGROUND

The term remote sensing is used for techniques, or a combination of techniques, which gather and process information without physical contact with the item or area of interest. In the electromagnetic regime, remote sensing detectors of various types cover a broad range from high energy gamma radiation down to low frequency radio. In the region of visible light, panchromatic imagery has been used for years to capture the reflected light from a scene and record the data on film. The platform for this remote sensor can be as simple as a hand-held camera or as complex as an orbiting satellite. Both provide a black and white photograph as a final product. Color photography covers the same spectral band as the panchromatic sensor, but does so multispectrally. Instead of recording light intensities for the entire visible band, color photography samples three portions which correspond to red, green and blue that the human eye can detect. The mixture of intensities of light for each band determines the shade of color that is subsequently portrayed on a photograph. This is a rudimentary form of multispectral imaging and other variations exist. Generally, multispectral imagers collect data from

several different bands which are not necessarily contiguous and can extend into the longwave infrared region. Hyperspectral sensors are a natural progression from multispectral and are generally intended for use from the ultraviolet spectrum to the infrared or a portion thereof. They collect information from a scene in hundreds of contiguous wavelength bands, extracting much more information from that scene than was previously possible. This permits discrimination of features and materials by measuring reflectance characteristics that would go otherwise unseen in a multispectral image. Theoretically, if the reflectance characteristic of an object is known, this object could be detected whenever its reflectance characteristic appeared in a scene. Spectra matching is one method used to detect and classify targets with hyperspectral imagery.

With the increased speed and capabilities of computers, the process of spectra analysis can be automated. This has significant implications for use by the military. With the sensor mounted on a satellite, UAV or an aircraft, a hyperspectral image can be taken of an area of interest. The data would be transmitted to a ground site where a computer would check for spectra matches for known targets of interest. Once detected, the computer would pass the type of target and geolocation through a data link to update the battlespace picture. This information can also be passed for use in cueing other sensors.

On the down side, the amount of data represented by one hyperspectral image is enormous. Dealing with data storage and transfers issues become a major concern. Additionally, data analysis takes longer with the larger data set. In a tactical scenario, time is of the essence and the faster a scene can be analyzed, from data collection to final output, the more useful hyperspectral imagery is to the warfighter. Thus it is important that analysis schemes and innovative systems architecture be devised which reduce the overall time from collect to dissemination of target locating data.

B. THESIS OBJECTIVES

The objective of this thesis is to describe a data collection and analysis scheme which would reduce data analysis requirements for hyperspectral imagery. The intent is to investigate the application of polarimetric data to deselect non-target regions and

thereby reduce the field of data which requires more thorough analysis. The viability of this application requires a study of the polarization characterization of objects to verify detectability of polarization differences.

C. THESIS OUTLINE

This thesis is divided into five chapters. The first chapter contains an introduction to the thesis. Chapter II provides background information regarding hyperspectral imagery including fundamental characteristics of reflected light, types of sensors, analysis techniques and proposed military application of hyperspectral imagery. Chapter III investigates polarization of reflected light to include polarization theory and recent studies regarding polarimetric characterization of targets. Chapter IV presents a hyperspectral data analysis scheme using polarimetry and presents designs for two proposed experiments to support the analysis technique. The first proposed experiment is designed to measure polarization characteristics of objects and backgrounds and investigate critical elements of the signature. The second proposed experiment attempts to investigate the applicability of polarization to hyperspectral analysis by collecting hyperspectral imagery of scenes with objects sampled during the first experiment. Chapter V lists conclusions and recommends future topics for possible research.

II. REMOTE SENSING

This chapter discusses remote sensing fundamentals, variations of instruments and future military applications. The characteristics of light are presented from a remote sensing perspective to include definitions of reflective and emissive electromagnetic spectrum, spectral variation of materials, interaction of light with the earth and its atmosphere and the geometry of reflected light. Spectral imaging sensors are described including fundamental analysis techniques. Finally, a proposed tactical remote sensing system is presented in an effort to provide a look at future requirements for remote sensing devices.

A. FUNDAMENTALS OF REMOTE SENSING

Different wavelengths of electromagnetic energy behave differently during interactions with varied materials and features, thus it is important to understand distinctions within the electromagnetic spectrum. As depicted by Figure 2.1, the electromagnetic spectrum extends from extremely low frequency radio all the way to gamma rays. While we normally characterize radio, television and microwave transmissions by their frequency, in the world of remote sensing, it is common to refer to electromagnetic waves by their wavelength.

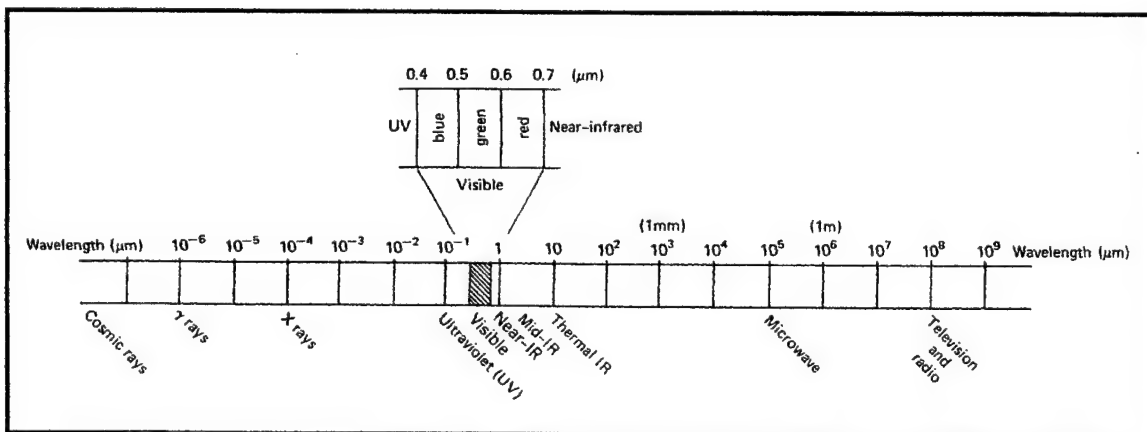


Figure 2.1: The Electromagnetic Spectrum. From Lillesand and Kiefer (1994).

1. Reflective and Emissive Bands

In general, light which can be observed by remote sensors may be divided into two bands consisting of reflected electromagnetic energy or emitted electromagnetic energy. Solar illumination is the dominant source of incident light for reflected energy, while the blackbody or thermal radiation inherent in the material is the primary source of emitted energy. For purposes of this thesis, the reflected energy band is of primary significance.

As shown in Figure 2.2, the region of reflected energy extends from 0.2 μm to 3.0 μm . This region contains the near ultraviolet band from 0.2 μm to 0.4 μm , the visible band from 0.4 μm to 0.7 μm , the near infrared or NIR band from 0.7 μm to 1.1 μm and the shortwave infrared or SWIR band from 1.1 μm to 3.0 μm . In the remote sensing community, the visible band is further divided into blue (0.4 - 0.5 μm), green (0.5 - 0.6 μm) and red (0.6 - 0.7 μm).

At 3 to 5 μm the spectrum consists of a mixture of solar reflected energy and thermally produced emitted energy. During the day, the midwave infrared region, or MWIR, is a region where both reflected solar energy and thermal emitted energy coexist. During the night, however, the solar source is no longer present and thermal sources dominate. Beyond 5 μm , thermal emissions always dominate. This is where the longwave infrared or LWIR band begins. Sometimes referred to as the emissive band, this region extends out to 14 μm .

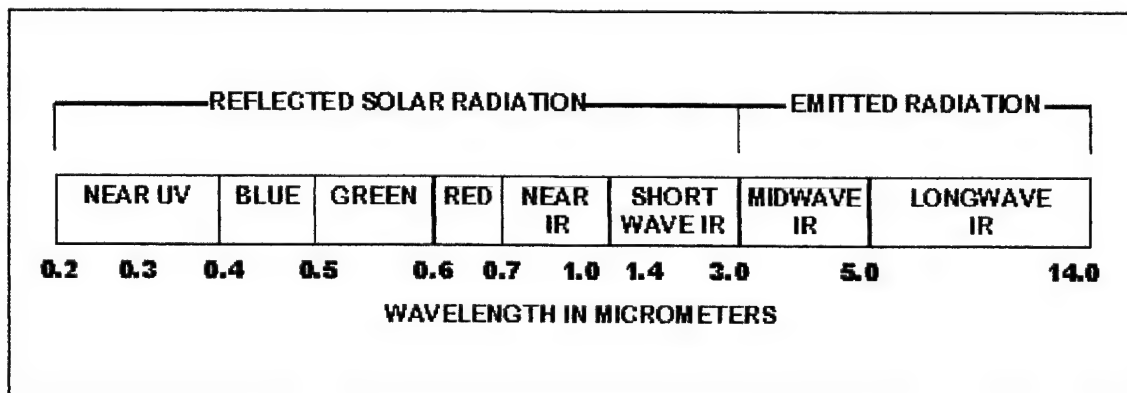


Figure 2.2: Spectral Regions.

2. Interaction of Light with Objects

When solar light interacts with an object on the Earth's surface, the energy will be reflected, absorbed and/or transmitted as shown in Figure 2.3. Based on conservation of energy, this can be expressed as

$$E_I(\lambda) = E_R(\lambda) + E_A(\lambda) + E_T(\lambda) \quad (2.1)$$

where E_I represents incident energy, E_R represents reflected energy, E_A is energy absorbed and E_T is transmitted energy.

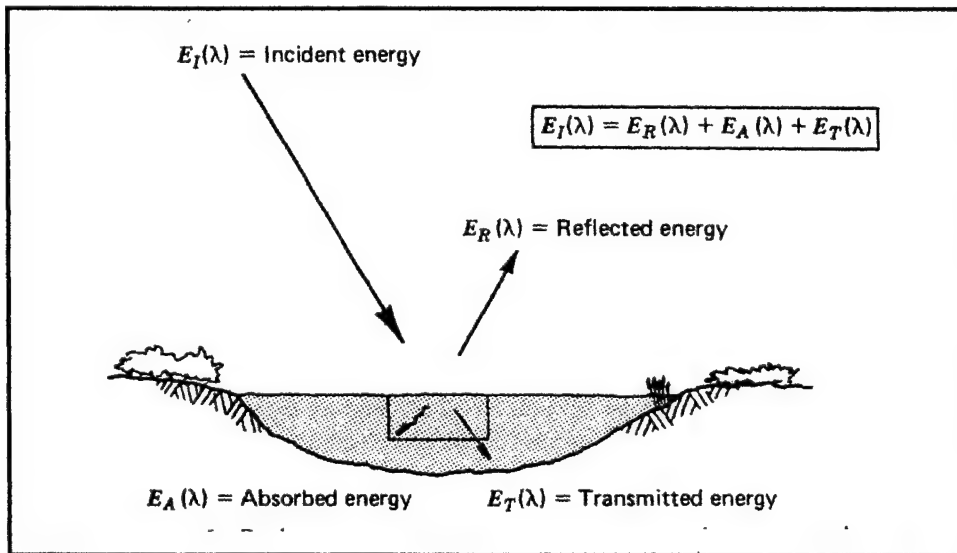


Figure 2.3: Basic Interaction of Light with the Earth's Surface. From Lillesand and Kiefer (1994).

The fraction of energy that is reflected, absorbed and transmitted will vary for different materials. This variability provides a means to differentiate one material from another and is most important for remote sensing. Since reflected energy is what is measured by most instruments, it is useful to rewrite Equation (2.1) as

$$E_R(\lambda) = E_I - [E_A(\lambda) + E_T(\lambda)] \quad (2.2)$$

For a given wavelength, Equation (2.2) shows that as incident light is decreased, the reflected light decreases as well, yet the proportions of light reflected, absorbed and transmitted remain the same. In a scene of varied illumination, such as would happen over varying terrain, similar materials will produce different brightness levels in direct proportion to the incident light as it varies with angle of incidence. A dimly lit material which ordinarily reflects very strongly at a particular wavelength may look similar to a more brightly lit material with a low reflectance value at that wavelength. Further, two materials may have the exact same values for reflected, absorbed or transmitted energy at a particular wavelength and will appear the same in this case as well.

Fortunately these values are wavelength dependent, meaning that the fractions of incident light that is reflected, absorbed or transmitted by a feature will vary throughout the spectrum and provides a remote sensing system with a method of distinguishing materials and features. The human eye is a multispectral imager that detects light in a range from 0.4 μm to 0.7 μm with three different sensitivities throughout this range. The collected intensities of light are transferred to the brain where they are combined to give color to an object. Thus, material which exhibits high reflection of red light will appear more red to the human eye. Likewise, material with a strong absorption coefficient in the same band will appear more green or blue depending on the coefficients for the remaining respective bands. In essence, the infinite spectral variation we see as color is a result of an infinite number of combinations of reflectance and absorptance coefficients.

3. Sources of Spectral Variation

Spectral variations are a result of the composition of the observed material. The composition can be characterized by the electronic, vibrational, and rotational resonant absorption in the material or feature. These absorption features are created by the transition of energy states within the atom or molecule. Transitions occur between electron energy levels in atoms and molecules and between vibrationally or rotationally excited states in molecules.

Electronic transitions create the line emissions seen in atoms and molecules by spectroscopy. When an atom transfers from an excited state to a state of lower energy, it

can decrease its energy by radiating a photon. The frequency of the emitted photon is directly proportional to the difference in energy levels as described by

$$E_x - E_y = \frac{hc}{\lambda} \quad (2.3)$$

where E_x is the higher energy state, E_y is the lower energy state, h is Planck's constant and λ is the wavelength of the emitted photon. Since a transition from a higher energy state to a lower emits a photon of a specific energy level, a photon arriving at the same energy level can be absorbed by the atom causing the electron to jump to a higher energy state. This phenomenon is described by Kirchoff's law which states that a body is exactly as good an absorber as it is an emitter.

The Lyman-alpha transition of atomic hydrogen is perhaps the most intense electronic transition emitter. This transition occurs between the first excited state and the ground state and is responsible for an intense UV solar line at 1216 angstroms. In general, when atoms are isolated, as in a gas, each atom is free to have its electrons at identical energy levels. As depicted in Figure 2.4, when interatomic spacing decreases, there is a splitting of the discrete energy levels into new levels associated with the collection of atoms. In the case of a molecule, a given energy state is split into several energy levels. When atoms are spaced even more closely, as in a solid, the split energy levels form a set of energy bands which in turn create bands of emitted light.

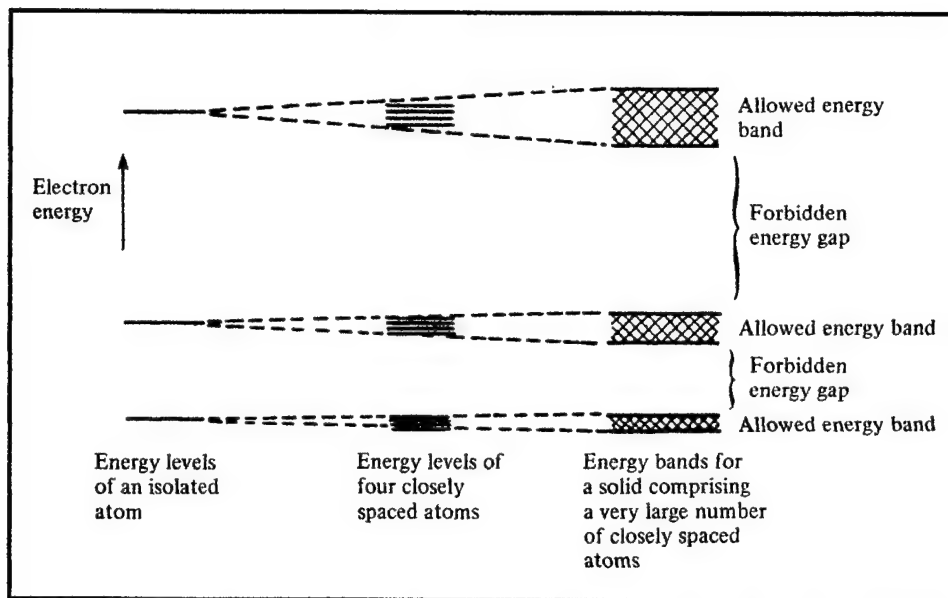


Figure 2.4: Schematic Representation of how the Energy Levels of Interacting Atoms form Energy Bands in Solids. From Wilson (1989).

Vibrational and rotational emissions are molecular in origin. They exhibit groups of closely spaced lines, with rotational emissions creating groups of lines with even narrower separation. As in the case described in Figure 2.4, vibrational and rotational emissions will create bands of emissions with the decrease in molecular separation. In the visible, near and midwave infrared region, absorption is caused by electronic transitions and molecular vibrational resonance. In the midwave and longwave infrared, molecular vibrational and rotational resonance are the dominating causes. Table 2.1 provides a list of characteristic spectra for solids.

Table 2.1: Characteristic Spectra of Solids. After Zissis (1993).

Type	Occurrence	Characteristic	Region
Crystal vibrations	Ionic crystals	Reststrahlen	15-300
Crystal vibrations on electronic transitions	Anions with rare earths or transition metals	Increased repetition of pattern	UV and visible
Free-electron oscillations	Metals	High reflectivity	Everywhere
Plasmas	Metals	Light spot	Everywhere
Unfilled shell transitions	4f, 5f, 3d, 4d, 5d	Sharp fluorescence	UV and visible
Color centers	Defects in ionic crystals	Absorption, coloring	UV and visible
Band-to-band transitions	Intrinsic semiconductors	Photoconduction	$h\nu > E_g$
Impurity transitions	Extrinsic semiconductors	Photoconduction	Everywhere
Free carriers	Semiconductors	Weak absorption	Everywhere

4. Spectral Reflectance

To understand the reflection characteristics of a material or feature, it is important to understand the source of incident radiation. Figure 2.5 shows a solar spectral irradiance curve. The upper solid curve represents solar irradiance at the top of the atmosphere. The dashed line represents an approximation of solar irradiance at the top of the atmosphere if the sun was a 6000K black body. The bottom curve represents the approximate solar radiation reaching the surface of the earth with losses due to absorption and scattering in the atmosphere. This bottom curve will vary depending on local atmospheric conditions, since local levels of aerosols, oxygen, ozone and water vapor all affect the amount of incident solar radiation that makes it to the earth.

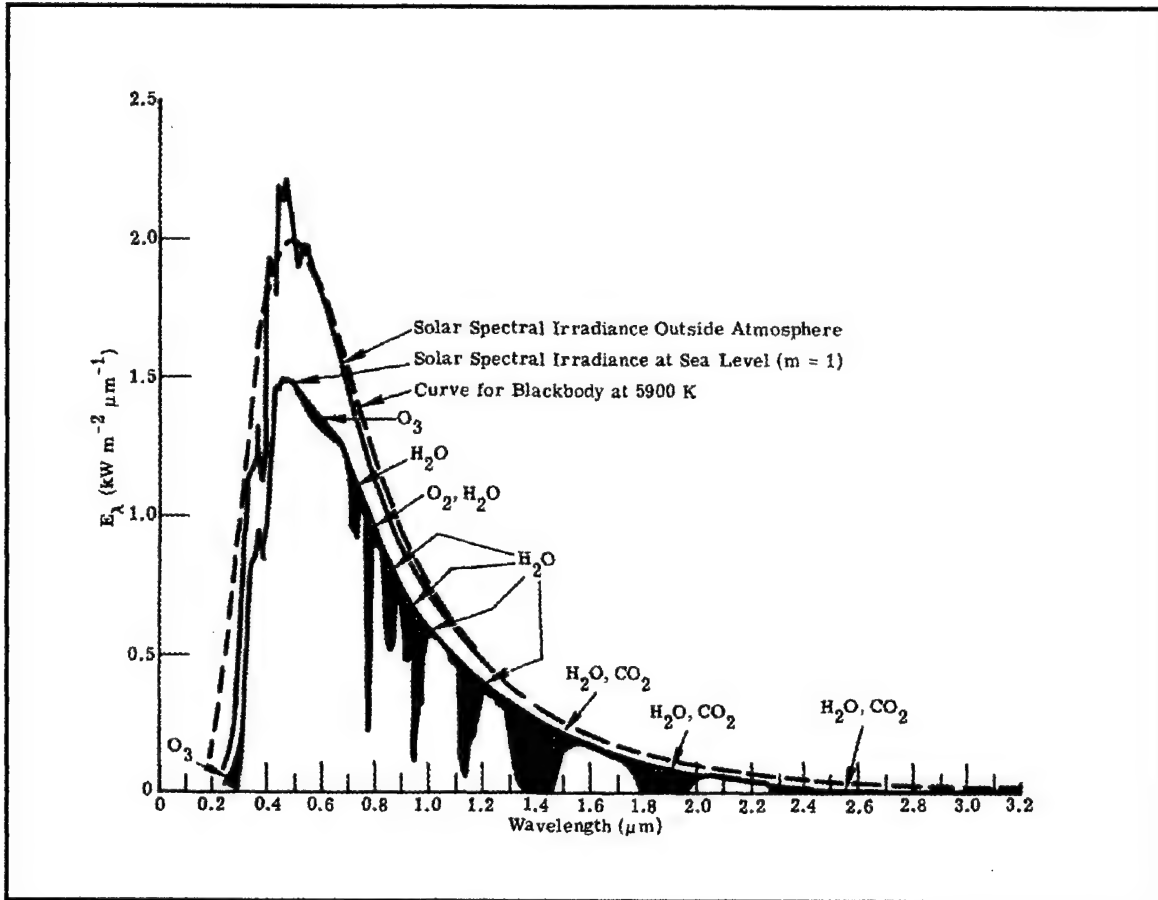


Figure 2.5: Solar Spectral Irradiance. From Zissis (1993).

When measuring reflected irradiance from a certain material, it should be recorded in a manner which minimizes variability. As previously discussed, solar irradiance is neither constant throughout the spectrum nor constant in location. One way to account for this variability in solar irradiance, is to describe the reflectance characteristic using spectral reflectance or ρ_λ . Spectral reflectance can be defined mathematically as

$$\rho_\lambda = \frac{E_R(\lambda)}{E_I(\lambda)} = \frac{\text{energy of wavelength } \lambda \text{ reflected from the object}}{\text{energy of wavelength } \lambda \text{ incident upon the object}} \quad (2.4)$$

By measuring both incident solar radiation and reflected radiation from an object simultaneously, the spectral reflectance value will be independent of any variation in

solar intensity. Thus a material will have the same spectral reflectance on a clear day as a cloudy or hazy day.

If spectral reflectance is measured for different wavelengths and subsequently plotted as a function of wavelength, the resulting curve is called a spectral reflectance curve. If we plot spectral reflectance as a function of wavelength for a number of different objects, we find that the shape of the curve differs from one object to another. This curve, in essence, maps out the color of the object. The profound implication is that the spectral reflectance curve can be used to identify an object and spectrally separate it from other objects. For example, Figure 2.6 contains a number of spectral reflectance curves for various construction materials. Notice the differences in reflectance values and also the way these values are distributed. It is this unique distribution of values that produces the color which the human eye can see and allows remote sensors a means to make material identifications.

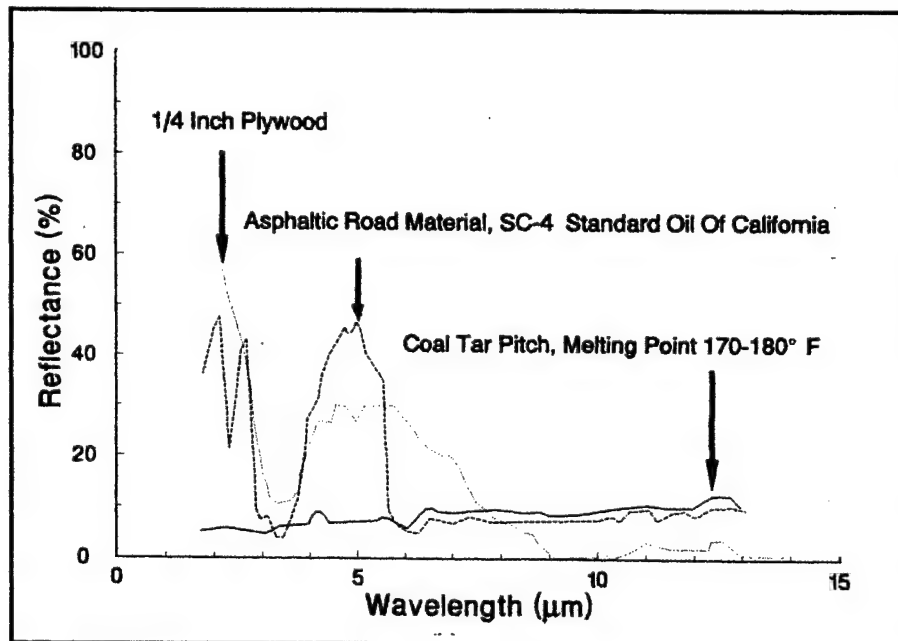


Figure 2.6: Spectral Reflectance Curves of Various Construction Materials.

From Zissis (1993).

As shown in Figure 2.5, solar irradiance is very different when measured at the top of the atmosphere compared to when it is measured at the earth's surface. While

Equation (2.4) automatically corrects for atmospheric absorption and its effect on the spectral variation of incident light, it does not compensate for atmospheric absorption features between the sensor and the object. When sampled very near to the object, the effects are minimal, but when a remote sensor is mounted on a satellite, atmospheric absorption becomes a large factor. Figure 2.7, shows absorption spectra for several molecular species including carbon monoxide, methane, ozone, water and carbon dioxide. As seen in this figure, atmospheric absorption features are many and varied.

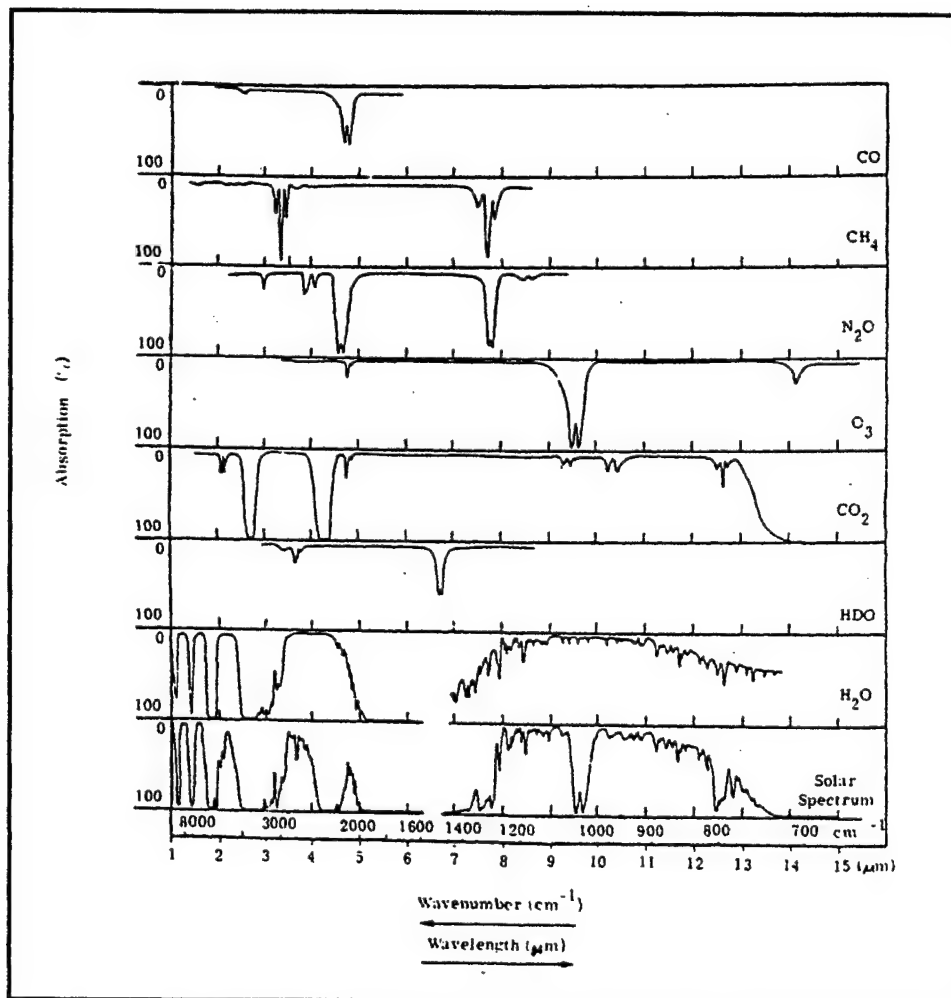


Figure 2.7: Atmospheric Absorption Spectra of Several Molecular Species. From Anderson et al (1994).

Complex radiative transfer equations and extensive compensation modeling have been created to correct for these variations. They will not be covered here, but it is important to understand that this form of compensation is often required in remote sensing and it is quite a complex problem.

5. Reflection of Light

The manner in which light is reflected can also be used to distinguish materials. The roughness or smoothness of the surface will impact the way light is reflected and gives the material texture. Light that is reflected by a perfect mirror is said to be specularly reflected; that is, a single incident beam of light produces a single reflected beam with equal angles of incidence and reflectance to the normal of the surface. When light is reflected uniformly in all directions, it is called a diffuse, isotropic or Lambertian reflection. Examples of specular and Lambertian reflection can be seen in Figure 2.8. Pure specular or Lambertian reflection does not normally occur in nature. Some combination of the two is more frequently observed.

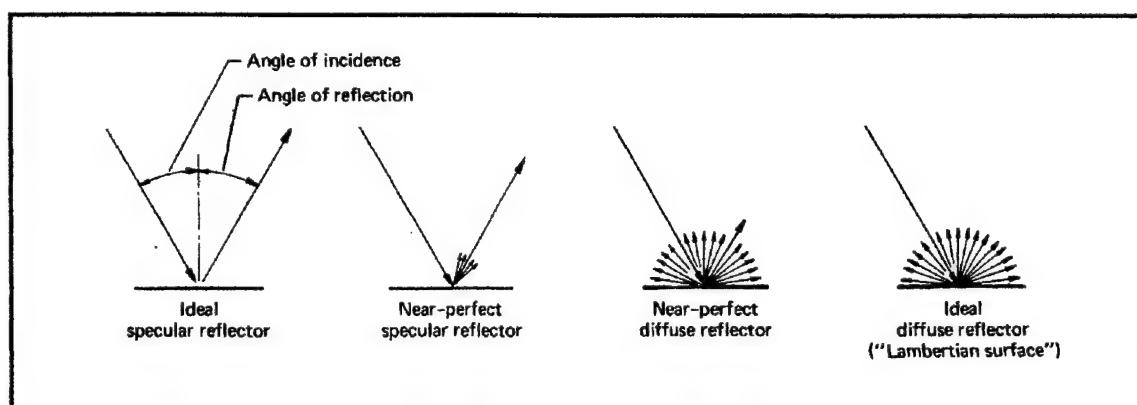


Figure 2.8: Basic Reflection Geometries. From Lillesand and Kiefer (1994).

For remote sensing purposes, it is important to note that specular reflectors will appear dark unless the sensor is aligned along the reflected beam. Lambertian reflectors, on the other hand, provide reflected light in all directions so that sensor positioning is not as critical. Because of this characteristic, remote sensing devices are normally designed to exploit Lambertian-type reflections.

As mentioned earlier, the manner in which light is reflected can be used for characterization. We viewed reflectance earlier as it depended on the wavelength, but it also depends on the angle of arrival of incident light, the angle of reflection and the polarization characteristics of the object. When the optical properties of an object or material are completely specified, the result is a bi-directional reflectance distribution function or BRDF. BRDF measurements are made using lasers in specially designed goniometric facilities which allow the laser, the sensor and the object to be rotated to measure reflectance at virtually any geometry. Studies for the effective use of BRDF for remote sensing applications is ongoing, but the almost infinite variations of geometries makes it very challenging indeed. (Anderson et al, 1994, pg. 2-8)

In summary, light useful for remote sensing is either reflected or emitted. For reflected light, the composition of an object or feature will determine the spectral variation of that reflected light. This spectral variation is useful in that it can be used to characterize a feature and therefore allow a system to distinguish that feature from others. One method of characterizing this is with spectral reflectance curves. Along with spectral variation, the surface roughness of the material can be determined based on the degree of diffusion of the reflected light.

B. SPECTRAL IMAGING

Spectral imagery consists of spatial data collected simultaneously from two or more spectral bands of the same scene. There are three major types of spectral imagery and these are categorized as multispectral, hyperspectral or ultraspectral. When describing spectral imaging devices, two specifications are frequently used to define the performance of the device. Spatial resolution is a property of the imager and refers to the resolving power of the instrument needed for the discrimination of feature, expressed as the smallest object dimension that can be detected by the sensor. Spectral resolution describes the sensor's imaging capabilities in terms of the spectral bandwidth, the number of spectral bands, and the location of those bands on the electromagnetic spectrum. Typically, the higher the spectral resolution, the narrower the bandwidth sampled.

As depicted in Figure 2.9, a multispectral sensor is sensitive to a series of bands which are relatively broad in range. Multispectral imagers generally collect less than ten spectral bands of a scene. LANDSAT, for example, is an eight band multispectral imager. Multispectral imagery allows spectral identification of major features like trees, roads and ground. Hyperspectral sensors collect images with higher spectral resolution, but on the order of hundreds of contiguous bands. This enables the sensor to detect subtle differences in signatures which can provide a means of discriminating between species of tree, types of road and moisture levels in the ground. Ultraspectral sensors look at very narrow bandwidths for thousands of bands and provide a means to discriminate extremely fine spectral details of materials, vapors and aerosols.

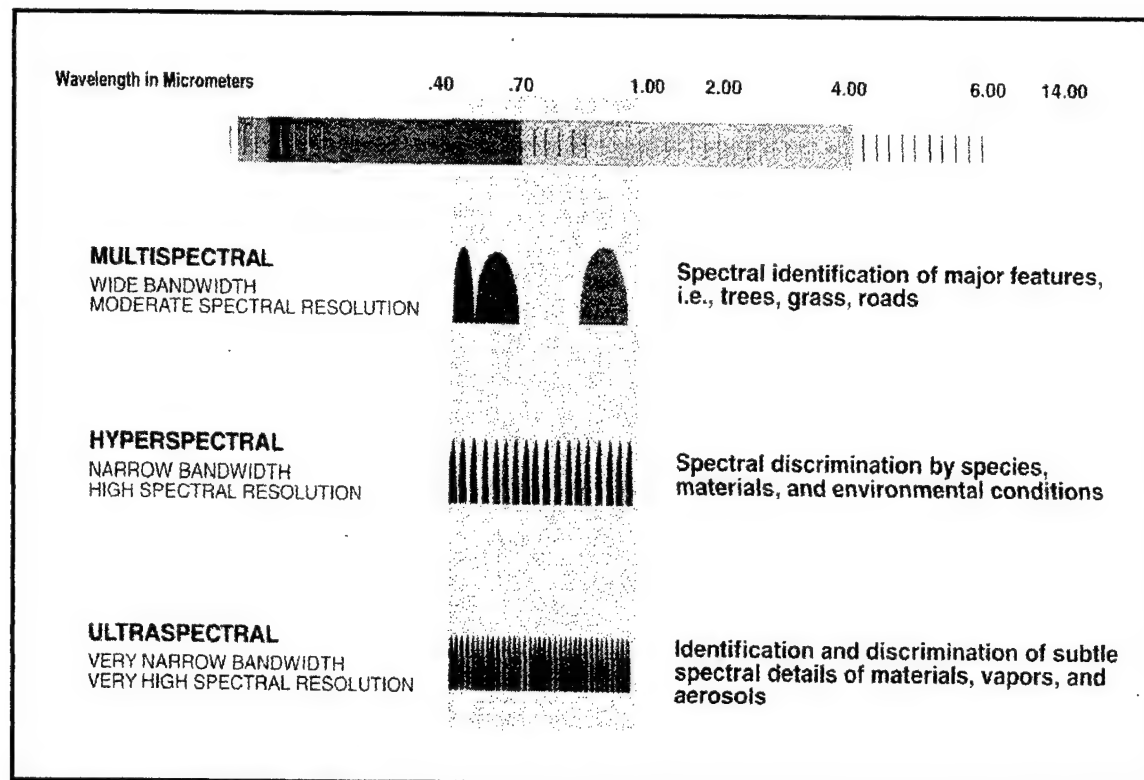


Figure 2.9: Types of Spectral Imaging. From Multispectral Users Guide (1995).

1. Hyperspectral Imagery

Hyperspectral imagery, or imaging spectroscopy, merges two remote sensing techniques; imagery and spectroscopy. This combination permits discrimination of features and materials within an imaged scene by measuring reflectance characteristics that would go otherwise unseen in a multispectral image. By collecting intensities of light with a contiguous set of narrow bands, the sensor is in essence developing spectral reflectance curves which can be analyzed one pixel at a time. If an object is spectrally characterized, a comparison of imaged spectral reflectance to a library signature can be conducted for each pixel in order to locate the object of interest within the image. Spectra matching is the term used to detect and classify targets with hyperspectral imagery. While efforts to develop viable Automatic Target Recognition (ATR) techniques for panchromatic imagery have met with limited success, ATR using hyperspectral imagery has proven much more successful.

When a hyperspectral image is taken of an area of interest, an entire image is collected for each and every band of the sensor. For instance, a 224 band hyperspectral imager would produce 224 band-specific images of the same scene. This collection of images defines a hypercube. The hypercube can be described by the two spatial dimensions normally seen in a photograph, with the added dimension of wavelength. As shown in Figure 2.10, each spatial element or pixel contains a continuous spectrum that represents the reflectance characteristics of everything in that pixel. Using spectra matching, each pixel can be analyzed to identify materials, equipment or other objects of interest. If the data hypercube is map registered, the object of interest can be assigned specific coordinates.

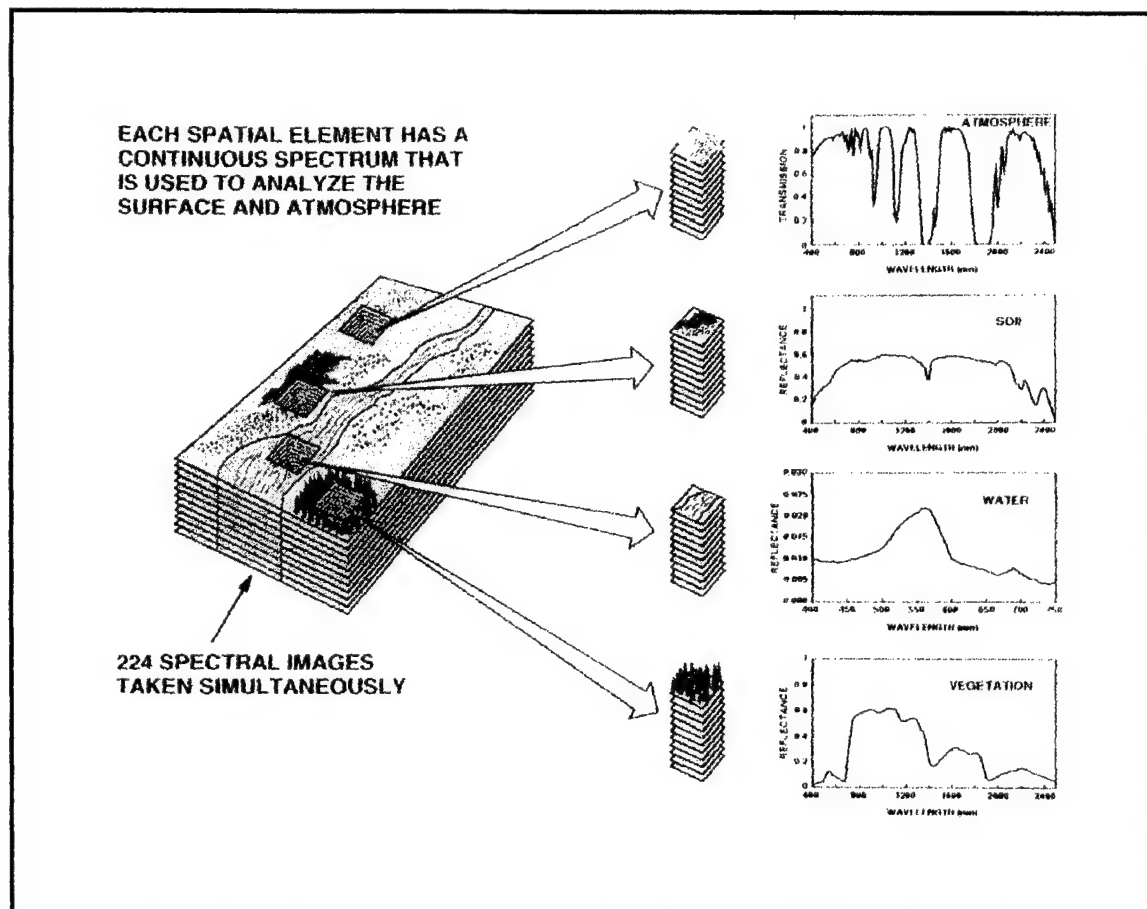


Figure 2.10: Hyperspectral Imaging Concept. From Multispectral Users Guide (1995).

In order to conduct spectra matching, however, the reflectance signature of an item of interest must be collected and stored in a signature file library. In a military sense, the signature library could contain reflectance characteristics of paints and metals used in military equipment, known effluents from weapon manufacturing or military equipment operation, camouflage netting and other materials. Additionally for intelligence preparation of the battlefield, a signature library could contain different types of vegetation, construction materials (wood, tin, steel, brick and concrete), road materials, and a variety of ground types from dry to soggy. All of this information would provide the military commander a better understanding of the playing field.

Hyperspectral imagery provides another benefit which was previously unattainable using traditional imagery techniques; unsupervised classification. With the increased speed and capabilities of computers, the process of spectra matching can be

automated. This has significant implications for use by the military. With the sensor mounted on a satellite, UAV or an aircraft, a hyperspectral image can be taken of an area of interest. The hypercube of data would be transmitted to a ground site where a computer would check for spectra matches for known targets of interest. Once detected, the computer would pass the type of target and geolocation through a data link to update the battlespace picture. This information can also be passed for use in cueing other sensors.

2. Basic Hyperspectral Imager Designs

The most fundamental component of a hyperspectral imager is the radiometric device. This device is responsible for measuring the levels of radiance or irradiance of an object. Hyperspectral sensors require a radiometer which is designed to allow determination of the wavelength distribution of radiation as well. There are three general ways to measure radiance as a function of wavelength; band pass filtering, spectroradiometry and interferometry. Another major component is the focal plane array which consists of an array of optical detectors situated at the focal plane of the instrument's optical path. These detectors may be thermal or photon devices. While there are a plethora of such detectors/sensors, the most commonly used detectors for imaging are charged coupled devices or CCD's.

Band pass filtering is a common method used in multispectral imagers, where only a limited number of bands are measured. The filters are normally laid out on the focal plane arrays and allow only the chosen wavelengths to fall on the detector. This technique of using individual band pass filters is not well suited to hyperspectral devices. Since the hyperspectral imager is required to collect hundreds of bands, this would therefore require hundreds of filters on a very small focal plane array. The Wedge Imaging Spectrometer uses a variation of the band pass filtering by use of a wedge shaped filter which achieves spectral separation of many bands using a single filter (Demro and Woody, 1993).

Spectroradiometers use dispersion to separate spectral components and achieve this through the use of prisms or diffraction gratings. The prism type device disperses

parallel rays of light into different angles from the prism according to wavelength as a result of refraction. This light is then collected by the detector. The grating type device accomplishes spectral separation through Fraunhofer diffraction and interference.

While these dispersive devices collect the entire spectrum simultaneously, they do not image an entire scene simultaneously. Instead, they gradually build the scene using either across-track (whiskbroom) scanning or along-track (pushbroom) scanning. As the name implies, whiskbroom scanners scan back and forth across the terrain while the aircraft or satellite traverses over the scene. As shown in Figure 2.11, these scanners collect spectral data from one point on the surface at a time by use of a rotating mirror which moves the instantaneous field of view across the flight path of the platform. This could be simulated by looking through a soda straw as you sweep across a scene. Although the optics are focused on what is effectively a single pixel, the focal plane array consists of a linear array of pixels totaling the number of spectral bands being sampled. As each pixel of spectral data is collected the data hypercube of the imaged scene slowly builds.

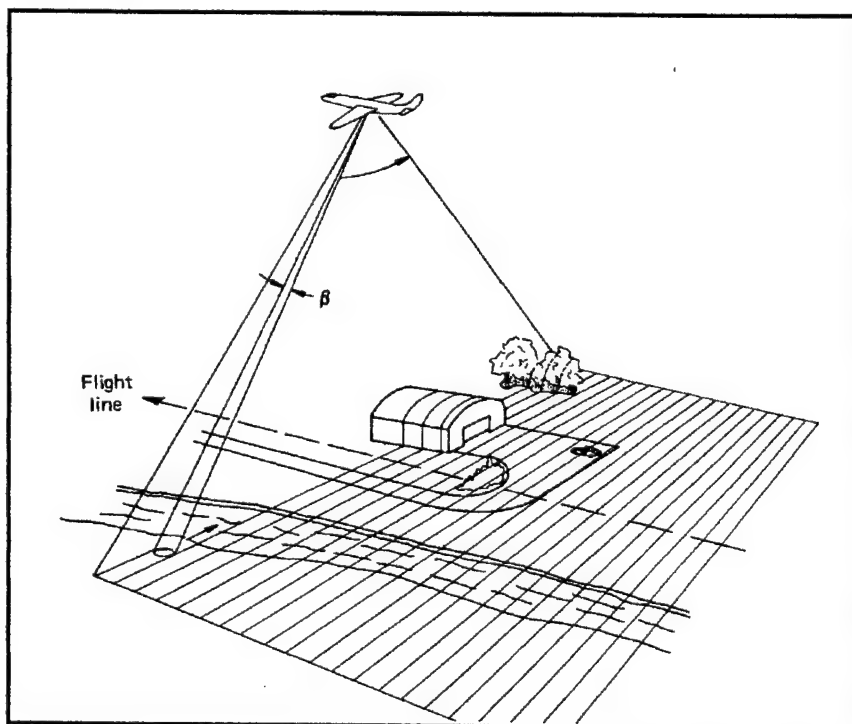


Figure 2.11: Whiskbroom Scanning. From Lillesand and Kiefer (1994).

Pushbroom scanners operate on the same idea, but this type of scanner looks at the scene through a slit many pixels wide as shown in Figure 2.12. Instead of a linear array with the total number of pixels equaling the number of spectral bands, the array is now two dimensional with one dimension determining the number of spectral channels to be collected and the second dimension determining the swath width. As it supports a larger instantaneous field of view, the pushbroom scanner can provide a faster sampling rate for the scene.

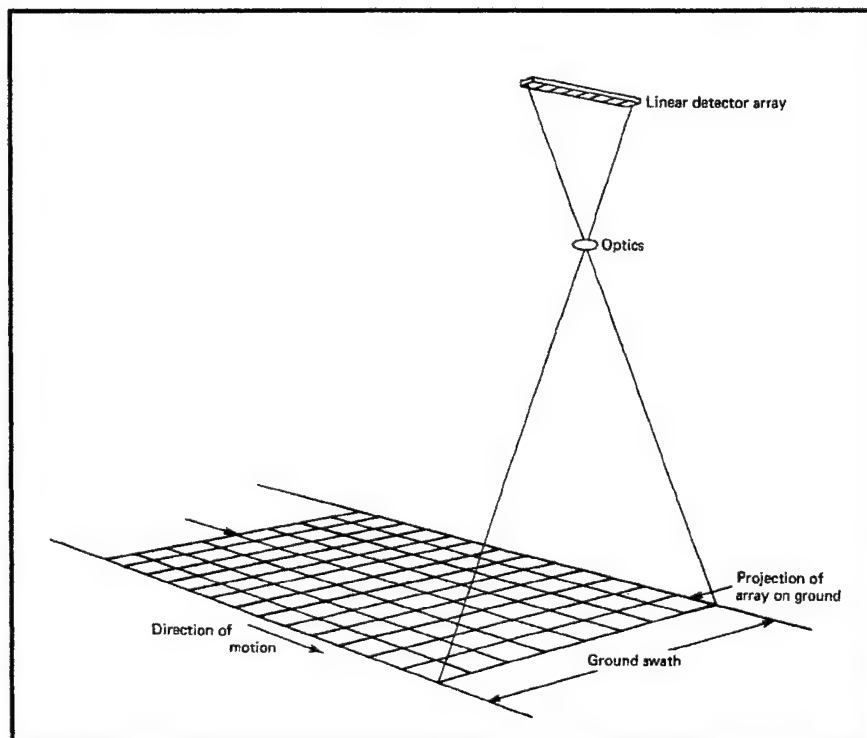


Figure 2.12: Pushbroom Scanning. From Lillesand and Kiefer (1994).

The third method to measure radiance as a function of wavelength is by use of an interferometer. Most common is the Imaging Fourier Transform Spectrometer (IFTS). While the dispersive system looks at spectral bands simultaneously and builds the scene by scanning, the IFTS images the entire scene and builds the spectrum that is sampled. The IFTS is based on the Michelson interferometer design which uses a moving mirror to sample interference patterns. The observed bandwidth is determined by the number of samples collected during the mirror stroke, while the length of the stroke determines the

spectral resolution. For hyperspectral applications the mirror motion is normally stepped which enhances the spectral accuracy. Unlike the scanning methods used by dispersive systems, IFTS devices are required to stare at the scene while each spectral image is collected.

C. MILITARY AND NATIONAL SECURITY INVOLVEMENT IN HYPERSPECTRAL SENSORS

Traditional image intelligence collection relies on pan-chromatic images and a human analyst to extract the important data from the image. This is a time consuming method of intelligence collection and is very often too slow for effective use in a continually changing tactical environment of a battlespace. Battlefield commanders have had to rely more on signals intelligence and a complex network of active sensors to rapidly update the battlespace picture. Attempts to automate the photo intelligence process have been met with limited success. Hyperspectral remote sensors, however, provide a possible means to speed up the image intelligence process. Automatic detection of items of interest through spectra matching and other analysis techniques would allow the warfighter to leverage off an already rapidly expanding C4I capability that the Information Age has produced, satisfying, however briefly, the need for faster flow on information. Controlling the battlespace entails complete knowledge of the battlespace. Hyperspectral sensors have received a great deal of attention from the military for that reason.

1. Description of Selected DoD Related Sensor Programs

a. HYMSMO Program

By far the most active program today is the Hyperspectral MASINT Support to Military Operations (HYMSMO) Program. According to a HYMSMO Program Office briefing paper (1993), this program is intended to sponsor a series of collection and exploitation experiments based on Operational Measurement and

Signatures Intelligence (OpMASINT) needs. The results of these studies will be used to assess the utility of hyperspectral sensors and provide acquisition recommendations for less complex, inexpensive OpMASINT prototype systems for development and testing. The overall goal is the procurement of an operational hyperspectral imaging system. This program is currently relying on experiments using the Naval Research Laboratory's Hyperspectral Digital Imagery Collection Experiment (HYDICE).

HYDICE was initiated in 1991 as a classified study to determine the utility of intelligence derived from hyperspectral imagery (Fay, 1995, p. 15). The instrument is an aircraft mounted nadir-viewing pushbroom device consisting of a Schmidt prism spectrometer with an Indium-Antimony (InSb) focal plane array. Spectral coverage ranges from 0.4 to 2.5 μm for the sensor which collects 206 contiguous bands with 10 nm spectral resolution.

The HYMSMO Program intends to use results from HYDICE experiments to demonstrate and advocate imaging hyperspectral systems as true MASINT resources due to their nonliteral imagery exploitation attributes and projected utility. Table 2.2 lists the candidate missions for hyperspectral imagery that will be evaluated. Additionally, the program intends to develop hyperspectral imagery exploitation algorithms and software to support quantitative utility assessments of HYMSMO and OpMASINT applications.

Table 2.2: Candidate HYMSMO Missions. After HYMSMO Program Office (1993).

• Camouflage, Concealment & Deception	• Locating and Mapping Land Mine Fields
• Battle Damage Assessment	• Locating & Identifying Amphibious Obstacles
• Safe Ingress/ Egress Routes, NBC Warfare	• Subsurface Structures Detection
• Safe Areas for Evasion and Escape	• Time Critical Target Detection & Identification
• Counter-Narcotics / Low Intensity Conflict	• Brilliant Weapons Target Signatures Refinement
• Terrain Mapping & Trafficability Analysis	• Non-Cooperative Target Identification

b. HRIS Program

Another non-commercial oriented program is the Hyperspectral Infrared Imaging Spectrometer Research Instrument (HRIS) being developed by the Department of Energy and Lawrence Livermore Laboratories. According to a HRIS Program Office briefing paper (1996), the HRIS instrument is intended to be an aircraft mounted imaging spectrometer that will operate in the long wave infrared (LWIR) with a spectral range of 7.8 - 12.5 μm . It uses a Fourier Transform Interferometer to collect 32 channels of spectral imagery on a 128 x 128 pixel array. For this instrument, the maximum stare time required is 3 seconds. The HRIS instrument is intended to measure spectral features of chemical effluence. While strategically important, this device is of limited use as a tactical sensor.

c. SEBASS Program

The Aerospace Corporation has sponsored the development and testing of the Spatially-Enhanced Broadband Array Spectrograph System (SEBASS). SEBASS is designed as a research instrument to explore the utility of hyperspectral infrared sensors for remotely identifying solids, liquids, gases, and chemical vapors in the 2 to 14 μm spectral region (Hackwell et al, 1996). The optical design uses the pushbroom collection scheme and relies on prisms for spectral dispersion. The focal plane array consists of two 128 x 128 pixel arrays, one for LWIR collection from 7.8 - 13.5 μm and the second for MWIR collection from 2.9 - 5.2 μm . When mounted on an aircraft the sensor is capable of spatial resolutions between 0.5 and 3 meters for aircraft altitudes between 1500 and 10,000 feet AGL. This technology offer substantial promise for target detection and defeat of CCD measures (Collins, 1996).

d. Warfighter-1 Program

At the Phillips Laboratory in Kirtland, New Mexico, the U.S. Air Force is currently working on a technical demonstration called Warfighter-1. The Space Experiments Directorate of the USAF Phillips Laboratory is responsible for performing enabling experiments and integration demonstrations to transition advanced space

systems related technology to the users. One of the directorate's programs, the Integrated Space Technology Demonstrations (ISTD) program, is tasked to find ways to correct Space Command deficiencies in the areas of space control, force enhancement and space support technologies related to warfighter needs. The goal of the program is to develop and test satellites capable of delivering real-time, mission essential data in various forms to the warfighter, even allowing the warfighter to directly control the satellite within the theater. Additionally, ISTD is exploring possible demonstrations of tactical remote sensing and imaging, space object identification, space object tracking, autonomous satellite control, missile warning, and Bomb Damage Assessment (BDA). The results of these demonstrations will help define requirements for possible use in future operational systems. Warfighter-1 is the first major technology demonstration for this program.

As described by the ISTD Program Office Statement of Requirements (1996), this system will consist of a satellite-mounted hyperspectral sensor which is controllable from a mobile mission ground site. When the satellite enters the theater airspace, the mobile mission ground site assumes command and control of the satellite, providing imagery tasking. Once collected, the data is transmitted directly to the mobile mission ground site for computer analysis. When detected using spectra matching, targets of interest and associated geolocation data will be transmitted to the C4I network. Thus a soldier in the field can open a laptop and get an updated picture of the battlespace as well as the military commander and staff. Additionally, autonomous cueing of other reconnaissance assets is desired. Tracking, telemetry and control (TT&C) of the satellite outside of the theater will be handled by a Fixed Ground Station. A general architecture is shown in Figure 2.13.

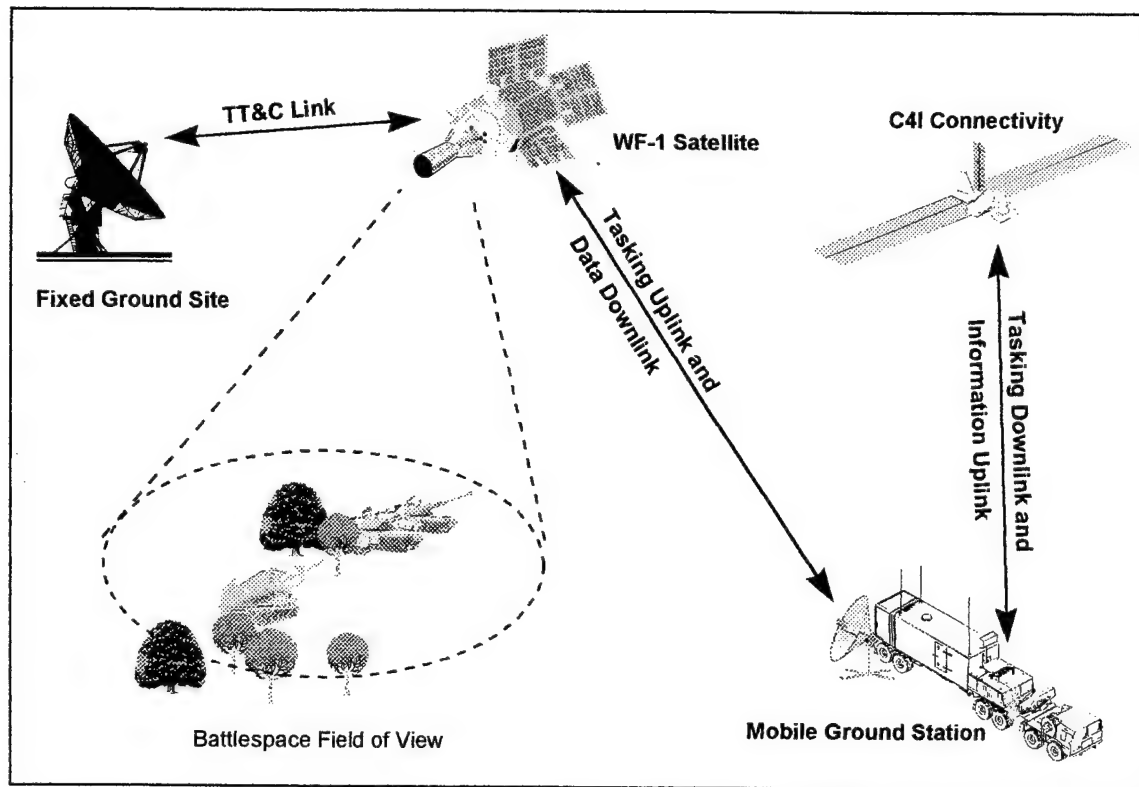


Figure 2.13: Warfighter-1 System Architecture.

2. Tactical Employment Challenges of the Warfighter-1

Warfighter-1 is intended to be a technology demonstration of the tactical employment possibilities of the hyperspectral imager. Therefore this program can be used to model the requirements for an operational system and reveal problem areas associated with a tactical hyperspectral sensor. As mentioned earlier, the major concern for use of hyperspectral data in a tactical environment is the amount of data that must be stored, transferred and analyzed. The Statement of Requirements for Warfighter-1 specified the imaging device to be a 60-plus band hyperspectral imager, optimized for the 0.4 to 2.5 micron band. In order to analyze link budget requirements, the following assumptions were made. The orbit would be sun-synchronous at an altitude of 600 km. The image would cover a swath 5 km wide and 20 km long with a ground resolution of 5 meters. 12 bit per pixel hypercube would be compressed using a 60% compression factor. Data analysis will only be accomplished at a Mobile Ground Station which would receive a direct downlink of the data from the WF-1 satellite. For illustration purposes

the satellite will be equipped with a 3 meter antenna and the Mobile Ground Station will receive using a large 6 meter mobile antenna.

Orbitology calculations indicate ground speed of the satellite to be 6.9 km/s with a 10 - 12 minute time in view. Given the swath size and ground resolution, each spectral band will be comprised of 4,000,000 pixels. A 60 band hypercube would contain 240,000,000 pixels. Using 12 bit digitization this translates to 2.88 Gbits of data. Using a 0.6 data compression factor, the cube can be reduced to 1.73 Gbits. The effect on the value of hyperspectral data after compression and decompression is a matter still under debate.

Assuming a carrier frequency of 7 GHz, altitude of 600 km, satellite antenna efficiency of 0.5, and an EIRP of 35 dBw, a data rate of 1.544 Mbps would require 18.7 minutes of transmission time to downlink the data hypercube. Since the maximum available time in view is 12 minutes, this is insufficient. Using a 12 Mbps data rate, similar to that of TDRS, gets the time required down to just 2.4 minutes. This should provide ample time to image the target area, process and compress the data and downlink the data cube to the Mobile Ground Station. Signal to Noise requirements for 16 QAM given a 10^{-6} bit error rate would be 18 dB. 64 QAM system would require 24 dB for the same BER. With a 6 meter antenna having an efficiency of 0.5, the received SNR is 37 dB and 46 dB respectively. This leaves more than enough overhead and would allow some antenna downsizing or allow the use of adaptive power.

Even though it is possible to image a scene and transfer a data hypercube to a mobile ground station within the time available, the system is limited to one scene per pass due to data transfer limitations. Some scheme must be developed which will speed this process up to allow multiple images. Secondly, once this data hypercube is received at the mobile ground station it must be analyzed. Methodology for hyperspectral data analysis remains a wide open field. Suffice to say, any technique which would reduce the data analysis time and provide key information to the C4I network quickly and accurately would be of great value to the tactical commander.

III. POLARIZATION

This chapter discusses the theory of polarization, examines sources of polarized light, conducts a review of polarization detection studies and provides a proposed application of polarimetric data for hyperspectral data analysis. The theory of polarization is first developed for electromagnetic waves where linear, circular and elliptical polarizations are described. The polarization state of light is addressed by describing methods of characterization using Stokes vectors and Mueller matrices. A section on sources of polarization examines Fresnel equations, reflection from conducting and non-conducting surfaces and selective absorption. Recent studies conducted on use of polarization for target detection are reviewed.

A. POLARIZATION STATE OF AN ELECTROMAGNETIC WAVE

Normally a beam of light consists of many individual electromagnetic waves, each with its own electric field vector oscillating in its own plane. When the orientation of these planes are uniform in distribution and the phase of electromagnetic waves are random, the light is considered unpolarized. Such is the case with solar radiance. If, however, a collection of electromagnetic waves traveling through free space has energy vectors which oscillate in a highly oriented manner, then the light is said to be polarized. There are three descriptions of polarized light; linear, circular and elliptical. Although linear and circular are actually special conditions of elliptically polarized light, it is convenient to characterize polarized light as such.

The electric field vector of an electromagnetic wave can be decomposed into two components with orthogonal electric fields. The following derivations are based on Guenther (1990). In complex notation the plane wave traveling along the z direction is described by

$$E = E_0 e^{i(\omega t - kz + \phi)} \quad (3.1)$$

Decomposing this equation into x and y components yields

$$E_x = E_{0x} e^{i(\omega t - kz + \phi_1)} = E_{0x} \cos(\omega t - kz + \phi_1) \quad (3.2)$$

$$E_y = E_{0y} e^{i(\omega t - kz + \phi_2)} = E_{0y} \cos(\omega t - kz + \phi_2) \quad (3.3)$$

Here the components differ in maximum amplitude and phase angle. Further, if the components are normalized, the equations are reduced to a pair of time dependent unit vectors varying as sinusoidals.

$$\frac{E_x}{E_{0x}} = \cos(\omega t - kz + \phi_1) = \cos(\omega t - kz) \cos \phi_1 - \sin(\omega t - kz) \sin \phi_1 \quad (3.4)$$

$$\frac{E_y}{E_{0y}} = \cos(\omega t - kz + \phi_2) = \cos(\omega t - kz) \cos \phi_2 - \sin(\omega t - kz) \sin \phi_2 \quad (3.5)$$

When plotted together at various values of ωt , the resulting curve forms an ellipse. The resulting curve is referred to as a Lissajous figure. To solve for an equation of the Lissajous figure, the frequency dependence ($\omega t - kz$) is removed by multiplying Equations (3.4) and (3.5) by $\sin \phi_2$ and $\sin \phi_1$ respectively then subtracting the two. Likewise the equations are multiplied by $\cos \phi_2$ and $\cos \phi_1$ and are again subtracted producing another pair of equations

$$\frac{E_x}{E_{0x}} \sin \phi_2 - \frac{E_y}{E_{0y}} \sin \phi_1 = \cos(\omega t - kz) (\cos \phi_1 \sin \phi_2 - \sin \phi_1 \cos \phi_2) \quad (3.6)$$

$$\frac{E_x}{E_{0x}} \cos \phi_2 - \frac{E_y}{E_{0y}} \cos \phi_1 = \sin(\omega t - kz) (\cos \phi_1 \sin \phi_2 - \sin \phi_1 \cos \phi_2) \quad (3.7)$$

If δ is used to represent the phase angle difference ϕ_1 and ϕ_2 , then

$$\cos\phi_1 \sin\phi_2 - \sin\phi_1 \cos\phi_2 = \sin(\phi_2 - \phi_1) = \sin\delta \quad (3.8)$$

After substituting $\sin\delta$ in the above equations, the two equations are squared and added together producing the Lissajous figure equation

$$\left(\frac{E_x}{E_{0x}}\right)^2 + \left(\frac{E_y}{E_{0y}}\right)^2 - \left(\frac{2E_x E_y}{E_{0x} E_{0y}}\right) \cos\delta = \sin^2 \delta \quad (3.9)$$

Thus the tip of the resultant electric field vector from the component vectors from Equations (3.6) and (3.7) traces out the polarization ellipse given by Equation (3.9).

1. Linear Polarization

One of two special cases of elliptical polarization, linear polarization occurs when the phase angle difference between two electric field vector components is 0 or π .

Substituting $\delta = 0$ into Equation (3.9) yields

$$\left(\frac{E_x}{E_{0x}}\right)^2 + \left(\frac{E_y}{E_{0y}}\right)^2 - \left(\frac{2E_x E_y}{E_{0x} E_{0y}}\right) = 0 \quad (3.10)$$

which can be reduced to

$$\left(\frac{E_x}{E_{0x}} - \frac{E_y}{E_{0y}}\right)^2 = 0 \quad (3.11)$$

and further to

$$\frac{E_x}{E_{0x}} = \frac{E_y}{E_{0y}} \quad (3.12)$$

In this case, the Lissajous equation resolves into a simple line equation $y = ax + b$ where the slope is E_{0y}/E_{0x} . When the phase difference is π , the slope is negative as shown in Figure 3.1.

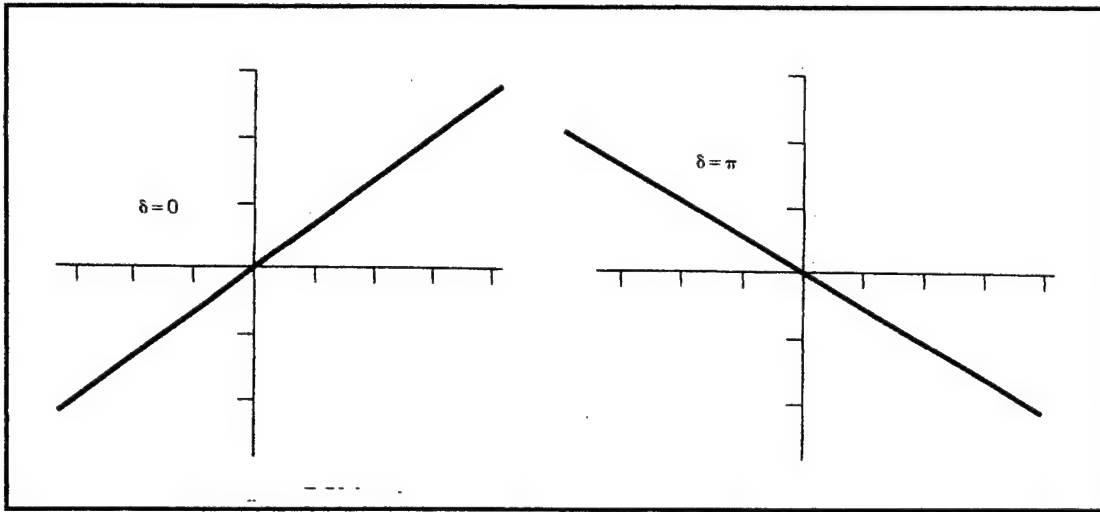


Figure 3.1: Lissajous Figure for Linearly Polarized Light. From Guenther (1990).

Additionally, the angle of the slope will vary as the maximum value of the electric field vector component changes. Thus at a fixed point in space, the electric field vector undergoes simple harmonic motion along the slope of the line defined by the maximum component vectors which are either in phase or 180° out of phase. This light is considered linearly polarized. Figure 3.2 shows the electric field vector in space at fixed time for linearly polarized light.

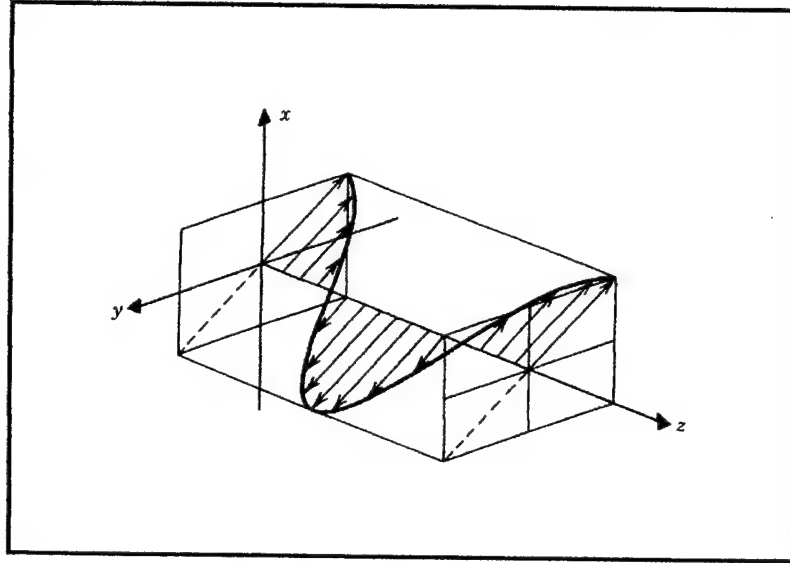


Figure 3.2: Representation of the Electric Field Vector in Space for Linearly Polarized Light. From Klein (1986).

2. Circular Polarization

In this special case of elliptical polarization the maximum amplitude for the electric field component vectors is the same for both axes. Additionally, the phase angle difference is plus or minus 90° , meaning that the x component leads or lags the y component by 90° . Again using the equation for the Lissajous figure given by Equation (3.9) and substituting $E_{0x} = E_{0y} = E$ and $\delta = \pm \pi/2$ produces

$$\left(\frac{E_x}{E_0}\right)^2 + \left(\frac{E_y}{E_0}\right)^2 = 1 \quad (3.13)$$

This is the normal conic form that defines the geometry of a circle with radius E_0 . As shown in Figure 3.3, in fixed space the resultant electric field vector rotates either clockwise or counterclockwise with the tip tracing out a circle.

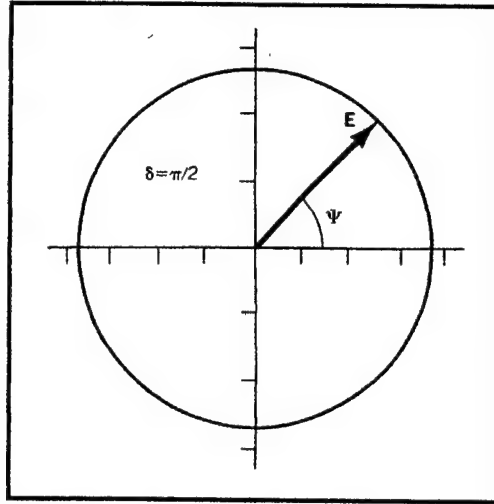


Figure 3.3: Lissajous Figure for Circularly Polarized Light. From Guenther (1990).

The directionality of the rotation is related to the sign of the phase difference between the x and y component vectors. When δ is a positive $\pi/2$, the rotation is clockwise and when δ is a negative $\pi/2$, the rotation is counter-clockwise. More common reference is to define the polarization as right-circularly polarized when it is rotating clockwise as it approaches the viewer and left-circularly polarized when rotating counterclockwise as it approaches the viewer.

3. Elliptical Polarization

The previous cases of linear and circular polarization are simply special cases of elliptical polarization. Figure 3.4 shows a plot of the resultant vector tip motion from Equation (3.9) where the amplitude of the electric field vector in the x direction is 0.75 and the amplitude for the y direction is 0.25. The two plots show the difference in slope of the major axis as determined by the phase difference.

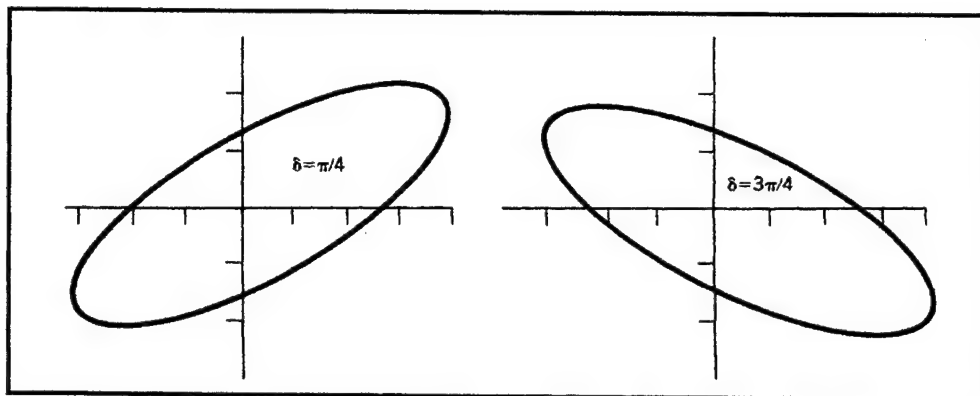


Figure 3.4: Lissajous Figures for Elliptically Polarized Light. From Guenther (1990).

In summary, an electromagnetic wave is composed of two orthogonal electric field components. The phase difference (δ) between the two components determines whether the wave is linearly or circularly polarized. When the phase difference is zero or π , the wave is linearly polarized. The ratio of component amplitudes determine the angle of the slope of the linear polarization. If the components are 90 degrees out of phase and the amplitudes are equal, the resultant wave is circularly polarized. Otherwise the wave is elliptically polarized.

B. POLARIZATION STATE OF LIGHT

While the polarization of an electromagnetic wave describes the character of individual waves, it is the collection of individual waves that determines the polarization of the light beam. An ordinary light source, such as the sun, consists of a large number of randomly oriented atomic emitters. Each excited atom radiates an electromagnetic wavetrain of a certain polarization. New polarized wavetrains are continually emitted by randomly oriented atoms, resulting in a beam of light which has no discernible polarization. This light is considered natural or unpolarized light. If the beam of light consists of a collection of waves similar in either phase or orientation of polarization, the beam of light is polarized. In reality, light is neither completely polarized nor unpolarized, but rather partially polarized, having polarized and unpolarized elements. The ratio of the flux density of the polarized portion to the flux density of the total

partially polarized light is defined to be the degree of polarization or P . The polarization characteristics of light can be expressed using Stokes vector notation. Using the notation of Nee (1995) this can be written as

$$\mathbf{S} = \begin{pmatrix} I \\ Q \\ U \\ V \end{pmatrix} = (I_u + I_p) \begin{pmatrix} 1 \\ P_L \cos 2\alpha \\ P_L \sin 2\alpha \\ P_C \end{pmatrix} \quad (3.14)$$

where

\mathbf{S} = Stokes vector (total flux density)

I = overall intensity

Q = intensity of polarized light oriented horizontally ($Q > 0$) or vertically ($Q < 0$)

U = intensity of polarized light oriented $+45^\circ$ ($U > 0$) or -45° ($U < 0$)

V = intensity of circularly polarized light for CW ($V > 0$) or CCW ($V < 0$)

I_u = intensity of unpolarized light

I_p = intensity of polarized light

P_L = degree of linear polarization

α = angle of linear polarization

P_C = degree of circular polarization

The degree of linear and circular polarization varies from 0 to 1 and satisfies the equation

$$P_L^2 + P_C^2 \leq 1 \quad (3.15)$$

When equal to 1, the beam of light is completely polarized.

While the Stokes vector characterizes the polarization state of a beam of light, it is useful to describe the change in character after the beam of light undergoes an interaction of some sort. A Mueller matrix is used to describe the optical properties of a material. The general form of the Mueller is

$$\mathbf{M} = \begin{pmatrix} A & C & 0 & 0 \\ C & B & 0 & 0 \\ 0 & 0 & D & F \\ 0 & 0 & -F & D \end{pmatrix} \quad (3.16)$$

Using this matrix, the Stokes vector output from an interaction of an incident beam of light (\mathbf{S}_0) with a medium described by the Mueller matrix (\mathbf{M}) is

$$\mathbf{S} = \mathbf{M}\mathbf{S}_0 \quad (3.17)$$

For example, a beam of unpolarized light interacts with the medium represented by the general form of the Mueller matrix. In this case, Q, U, and V for the incident Stokes vector are equal to zero. Multiplying by the Mueller matrix produces

$$\mathbf{S} = \begin{pmatrix} A & C & 0 & 0 \\ C & B & 0 & 0 \\ 0 & 0 & D & F \\ 0 & 0 & -F & D \end{pmatrix} \cdot \mathbf{I} \begin{pmatrix} 1 \\ 0 \\ 0 \\ 0 \end{pmatrix} = \mathbf{I} \begin{pmatrix} A \\ C \\ 0 \\ 0 \end{pmatrix} \quad (3.18)$$

Thus the unpolarized light becomes linearly polarized. Since the degree of linear polarization is equal to the ratio of polarized flux density to total flux density, it follows that the degree of linear polarization in this case is C/A . This ratio represents the capacity for the medium to convert unpolarized light to polarized light.

Given an incident beam of light which is linearly polarized at 45° or $\pi/2$, the resulting beam of light would become

$$\mathbf{S} = \begin{pmatrix} A & C & 0 & 0 \\ C & B & 0 & 0 \\ 0 & 0 & D & F \\ 0 & 0 & -F & D \end{pmatrix} \cdot \mathbf{I} \begin{pmatrix} 1 \\ 0 \\ 1 \\ 0 \end{pmatrix} = \mathbf{I} \begin{pmatrix} A \\ C \\ D \\ -F \end{pmatrix} \quad (3.19)$$

producing elliptically polarized light with a degree of circular polarization of $-F/A$.

The values for the Mueller matrix of a particular medium are normally measured using ellipsometry (Nee, 1995, p. 221). Knowing the character of the incident beam of light and carefully measuring the resultant beam after an interaction provides the data necessary to estimate the composition of the Mueller matrix. The Mueller matrix then describes the polarization characteristic of the object. While the matrix represents the overall polarization characteristic of an object, it can also be used to define polarimetric response for a particular wavelength or set of wavelengths. In this case the equation could be rewritten

$$\mathbf{S}_\lambda = \mathbf{M}_\lambda \mathbf{S}_{0\lambda} \quad (3.20)$$

This dependency on wavelength allows for the possibility of the variability of the polarimetric response of a medium or object throughout the spectrum of incident radiation.

C. SOURCES OF POLARIZATION

Polarized light can be created in many different ways depending on the optical properties of the material either reflecting or emitting the polarized light. Perhaps the most prevalent polarizer is reflection, where light that is oriented normal to the plane of incidence is preferentially reflected compared to light which is oriented along or parallel to the plane of incidence. Absorption will create polarized light when the optical properties of the material absorbs light of a particular orientation and reflects the other.

Additionally, light may become polarized through interference patterns produced by the material, destructively interfering with a particular orientation. Some types of crystalline material have different indices of refraction within the material depending on orientation and will produce a polarizing effect through what is known as birefringence. Lastly, the plane of polarization may be rotated by optically active material. This material, crystalline, gaseous or liquid, possesses mirror image molecules which create the rotation effect.

The effects of polarization by interference, birefringence and optical activity are normally observed in the transmission of light, which is useful in designing optical polarizers. In consideration for use in spectral characterization of material and features, however, the most applicable are reflection and absorption polarization.

1. Fresnel Equations

When a light wave interacts with a material, the light is either reflected from or transmitted into the material where it is either absorbed, scattered or transmitted through the medium. When measured from a line normal to the material, light that is reflected will be reflected at the same angle as represented by the Law of Reflection

$$\sin \theta_i = \sin \theta_r \quad (3.21)$$

where θ_i is the angle of incidence and θ_r is the angle of the reflected ray. However, that portion of light that is transmitted experiences refraction. This refraction of light is due to the change in index of refraction between the two mediums. Quite simply, the index of refraction is a ratio of the speed of light in free space to the speed of light within the medium or material is

$$n = \frac{c}{v} = \sqrt{\frac{\epsilon\mu}{\epsilon_0\mu_0}} \quad (3.22)$$

where n is the index of refraction, c is the speed of light in a vacuum, v is the speed of light in a medium, ϵ and ϵ_0 are the dielectric constants for the medium and a vacuum respectively and μ and μ_0 are the permeability constants for the medium and vacuum. The Law of Refraction, or Snell's Law, describes the transmission of light through a change in indices of refraction by

$$n_1 \sin \theta_i = n_2 \sin \theta_t \quad (3.23)$$

where n_1 and θ_i represent the index of refraction of the first medium and the angle of incidence respectively and n_2 and θ_t represent the index of refraction of the second medium and the angle of refraction. Additionally, there is a wavelength dependence for the velocity of an electromagnetic wave through a medium which in turn causes the index of refraction vary with wavelength. It is this wavelength dependence which allows a prism to chromatically disperse a beam of light.

When applied to the interaction between light and some medium or material, the law of Conservation of Energy requires that the combined energy of reflected, absorbed and transmitted light equals that of the incident light. As discussed above, the laws of reflection and refraction describe the geometry of this interaction, but they do not describe the effect on the amplitude of the light. The boundary conditions of Maxwell's equations places a dependence on the orientation of the incident wave and thus the polarization with respect to the incident plane, thus affecting the reflected and transmitted waves differently depending the polarization of the waves.

To describe the interaction in terms of amplitude requires that the cases of perpendicular and parallel polarization be solved separately. This is achieved by using Fresnel equations which solve for the amplitude coefficients for reflection and transmission for each of the polarizations. The amplitude coefficients represent the degree to which the amplitude of the incident electric field vector is affected in the interaction such that

$$E_r = \rho_{12} E_i \quad \text{and} \quad E_t = \tau_{12} E_i \quad (3.24)$$

In the case of oblique incident electromagnetic waves with an electric field vector perpendicular to the plane of incidence, the amplitude reflection and transmission coefficients are

$$\rho_s = \left(\frac{E_r}{E_i} \right)_s = \frac{n_1 \cos \theta_i - n_2 \cos \theta_t}{n_1 \cos \theta_i + n_2 \cos \theta_t} \quad (3.25)$$

$$\tau_s = \left(\frac{E_t}{E_i} \right)_s = \frac{2n_1 \cos \theta_i}{n_1 \cos \theta_i + n_2 \cos \theta_t} \quad (3.26)$$

In the case of oblique incident electromagnetic waves with an electric field vector parallel to the plane of incidence, the amplitude reflection and transmission coefficients are

$$\rho_p = \left(\frac{E_r}{E_i} \right)_p = \frac{n_2 \cos \theta_i - n_1 \cos \theta_t}{n_2 \cos \theta_i + n_1 \cos \theta_t} \quad (3.27)$$

$$\tau_p = \left(\frac{E_t}{E_i} \right)_p = \frac{2n_1 \cos \theta_i}{n_1 \cos \theta_t + n_2 \cos \theta_i} \quad (3.28)$$

By invoking Snell's law, Equation (3.23), the Fresnel equations can be rewritten as

$$\rho_s = -\frac{\sin(\theta_i - \theta_t)}{\sin(\theta_i + \theta_t)} \quad (3.29)$$

$$\rho_p = \frac{\tan(\theta_i - \theta_t)}{\tan(\theta_i + \theta_t)} \quad (3.30)$$

$$\tau_s = \frac{2 \sin \theta_t \cos \theta_i}{\sin(\theta_i + \theta_t)} \quad (3.31)$$

$$\tau_p = \frac{2 \sin \theta_t \cos \theta_i}{\sin(\theta_i + \theta_t) \cos(\theta_i - \theta_t)} \quad (3.32)$$

Normally what is measured from an interaction is not the electric vectors, but the intensity or average energy flux per unit area. This intensity can be described by the magnitude of the Poynting vector

$$\bar{S} = \frac{1}{2} \frac{n}{\mu_o c} (E_p^2 + E_s^2) \quad (3.33)$$

where E_p and E_s represent the amplitudes of the electric field vector parallel and normal to a given reference, in this case, the incident plane. Further, the ratio between the reflected flux density and the incident flux density is defined as reflectance

$$R = \frac{S_r}{S_i} \quad (3.34)$$

Likewise the ratio of the transmitted flux density to the incident value is defined as transmittance

$$T = \frac{S_t}{S_i} \quad (3.35)$$

Combining Poynting vector relationship, Equation 3.32, with Equation 3.23 and the Fresnel coefficients gives reflectance and transmittance values for both polarizations as

$$R_s = \rho_{12s}^2 \quad T_s = \frac{n_2 \cos \theta_t}{n_1 \cos \theta_i} \tau_{12s}^2 \quad (3.36)$$

$$R_p = \rho_{12p}^2 \quad T_p = \frac{n_2 \cos \theta_t}{n_1 \cos \theta_i} \tau_{12p}^2 \quad (3.37)$$

To satisfy conservation of energy, the identities $R_s + T_s = 1$ and $R_p + T_p = 1$ must hold true for oblique incidence on a non-conducting material.

These equations apply to a specific wavelength for any linear, isotropic, homogeneous material which behaves as a dielectric. They do not represent the polarimetric response of a material due to variation of the material's index of refraction as a function of wavelength. Nor do they account for a complex index of refraction. It can be argued that the values for the Fresnel coefficients, which depend on the index of refraction, may vary with wavelength and the resulting polarimetric response to the interaction will exhibit a wavelength dependency as well.

2. Reflection from a Non-conducting Material

Equations (3.36) and (3.37) can be plotted as a function of the angle of incidence. The resulting curves are as depicted by Figure 3.5 for s-polarized waves and Figure 3.6 for p-polarized.

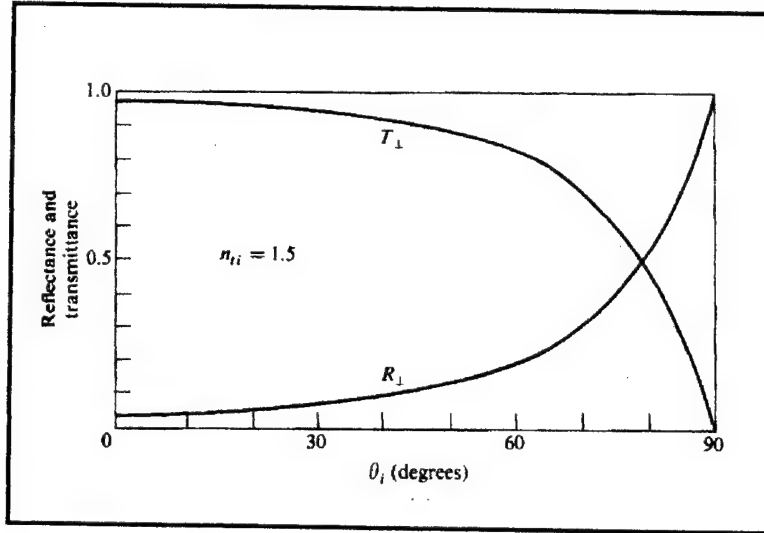


Figure 3.5: Reflectance and Transmittance versus Angle of Incidence for Perpendicular Polarizations. From Hecht (1989).

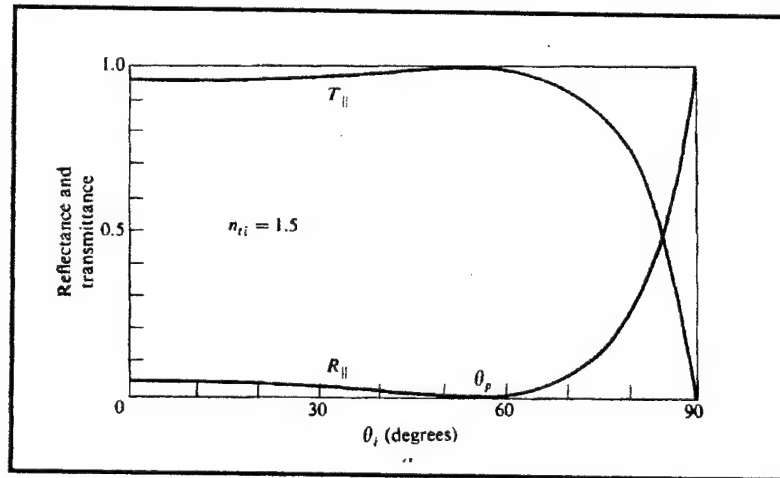


Figure 3.6: Reflectance and Transmittance versus Angle of Incidence for Parallel Polarizations. From Hecht (1989).

The reflectance curve for the s-polarized wave shown in Figure 3.5 shows an increase of reflectance with increasing angle of incidence. At high angles of incidence the reflectance is very large. The reflectance curve in Figure 3.6 for the p-polarized wave, however, goes to zero at one point, then begins an upward trend with large reflectance at high angles of incidence. From Equation (3.29) for the reflection coefficient of the p-polarized wave, the value of the coefficient is zero when $\tan(\theta_i + \theta_t) = \infty$. This will

occur whenever $\theta_i + \theta_t = \pi/2$. Since the s-polarized wave is partially reflected, unpolarized light incident with this condition will become polarized after the interaction as shown in Figure 3.7. The angle of incidence where this occurs is known as Brewster's angle.

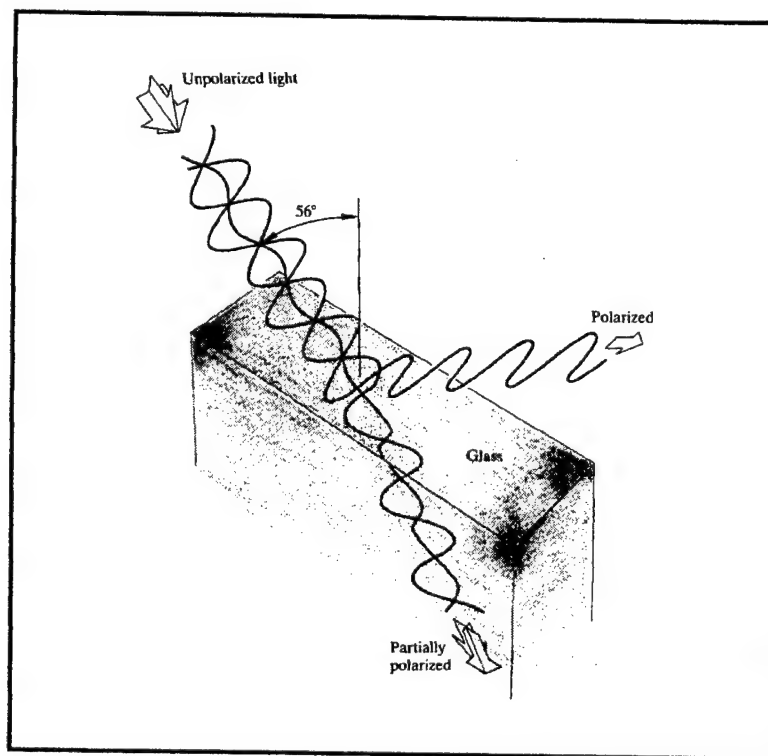


Figure 3.7: Polarization of Light Due to Reflection at Brewster's Angle.

From Hecht (1989).

To solve for Brewster's angle, Snell's law (Equation (3.23)) is used by substituting

$$\theta_t = \frac{\pi}{2} - \theta_i$$

into Snell's law, which yields

$$n_1 \sin \theta_B = n_2 \sin \left(\frac{\pi}{2} - \theta_B \right) = n_2 \cos \theta_B$$

which can be reduced to a function of the tangent producing Brewster's law

$$\tan \theta_B = \frac{n_2}{n_1} \quad (3.38)$$

The reflectance curves from Figures 3.5 and 3.6 are drawn on the same plot in Figure 3.8 and clearly shows the preferential reflection of the s-polarized wave over the p-polarized wave. In this case the curves represent an air-glass interface where Brewster's angle is 56° .

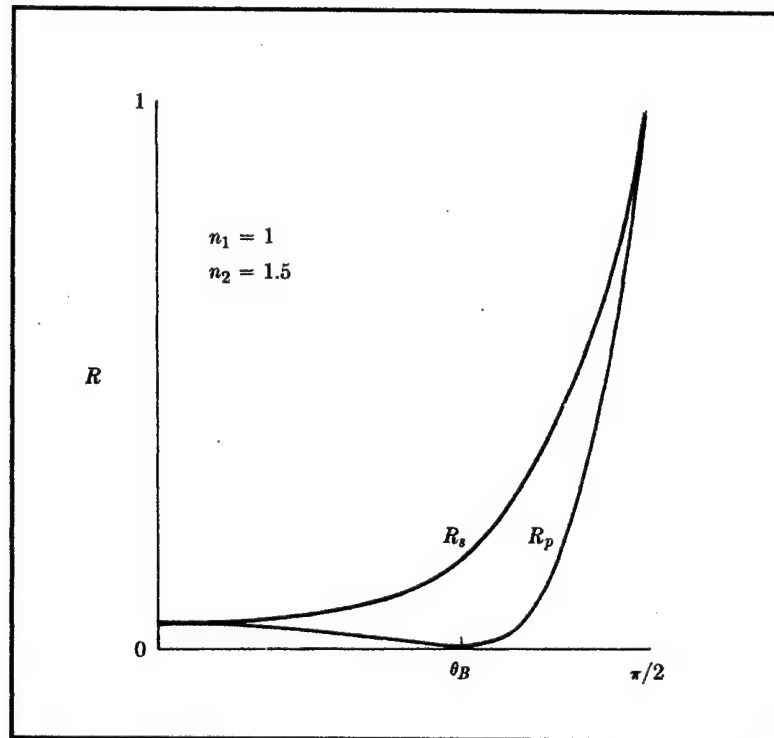


Figure 3.8: Reflectance for S- and P-polarized Waves at an Air-glass Interface. From Reitz (1993).

3. Reflection from a Conducting Material

Unlike a dielectric material, a conducting material features free electric charges in the form of electrons. These electrons are free to circulate within the material and with that motion produce current. Ohm's law relates the resultant current per unit area to the application of an electric field as

$$\mathbf{J} = \sigma \mathbf{E} \quad (3.39)$$

where \mathbf{J} is the current density and σ represents the conductivity of the material. In the case of a dielectric, there are no free electrons available to produce current and therefore the conductivity is zero ($\sigma = 0$). In conducting materials, such as metals, the conductivity has a finite non-zero value. Taken to the extreme, a perfect conductor would have a conductivity value of 1 and all applied electric fields would simply propagate through the media as electrons. In real conductors, the electrons undergo collisions with the thermally excited lattice structure of the material as well as imperfections in the lattice effectively converting electromagnetic energy to heat. This conversion is referred to as absorption.

Since all the energy transmitted into a conducting medium is eventually absorbed, absorptance is defined as

$$A = 1 - R \quad (3.40)$$

This property of absorption complicates the solution of Fresnel's equations. Recall from Equation (3.22) that the index of refraction is

$$n = \sqrt{\frac{\epsilon \mu}{\epsilon_0 \mu_0}}$$

In general, n can be complex. The complex form of the dielectric constant is

$$\tilde{\epsilon} = \epsilon - i\left(\frac{\sigma}{\omega}\right) \quad (3.41)$$

In a non-conducting medium conductivity is zero, therefore the imaginary portion goes to zero and only a real value remains for the dielectric constant. In the case of conductors, however, the imaginary portion must be considered, resulting in a complex index of refraction. It is important to note that the imaginary portion of the dielectric constant has a wavelength dependency which makes it possible for the index of refraction for a conducting material to vary with wavelength as shown in Figure 3.9.

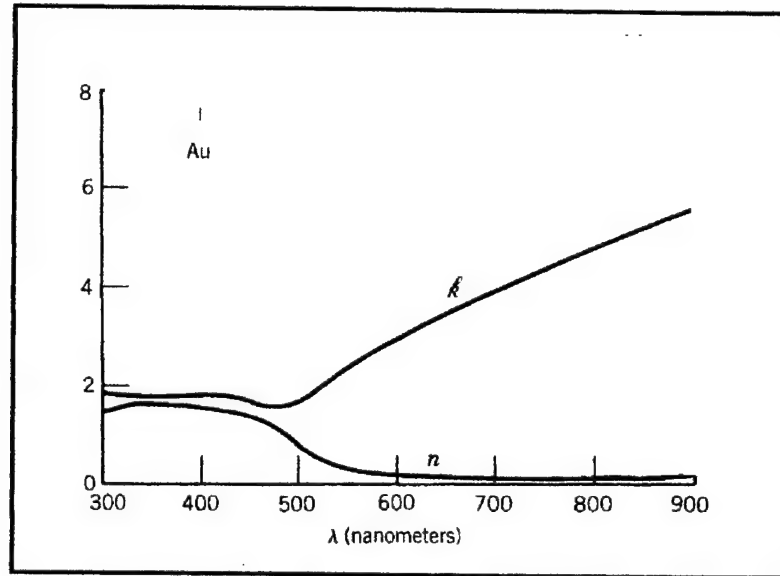


Figure 3.9: Real (n) and Imaginary (k) Parts of the Complex Index of Refraction for Gold. From Klein (1986)

For the relatively simple case where the angle of incidence is near normal for an air to metal interaction, Equation (3.27) becomes

$$\rho_N = \frac{n_2 - n_1}{n_2 + n_1} \quad (3.42)$$

and when substituted into Equation (3.26), reflectance becomes

$$R_N = \left(\frac{n_2 - n_1}{n_2 + n_1} \right)^2 \quad (3.43)$$

Substituting $n_1 = 1$ for air and $n_2 = n + i k$ for the complex index of refraction for a metal the result is

$$R_N = \left(\frac{n - 1 + k}{n + 1 + k} \right) \left(\frac{n - 1 - k}{n + 1 - k} \right) \quad (3.44)$$

which further reduces to

$$R_N = 1 - \frac{4n}{(n + 1)^2 + (k)^2} \quad (3.45)$$

or by Equation (3.40)

$$A_N = \frac{4n}{(n + 1)^2 + (k)^2} \quad (3.46)$$

When the imaginary value becomes very large while the real value remains relatively small, absorptance values become very small and conversely, reflectance values become very large. If the index of refraction was purely imaginary, the material would exhibit total reflection of light.

Plotting the oblique incidence reflectance for p- and s-polarized waves, as shown in Figure 3.10, shows a similar relationship to that of a non-conducting interaction. While reflectance value for the p-polarized wave drops as before, the minimum is no longer zero and there is no Brewster's angle where the reflectance goes to zero. This

minimum point, however, is known as the principle angle of incidence. The polarization effect resulting from an interaction with a conducting surface still preferentially reflects s-polarized incident waves at the expense of p-polarized waves resulting in a partially polarized beam of light which is dominated by s-polarized electromagnetic waves.

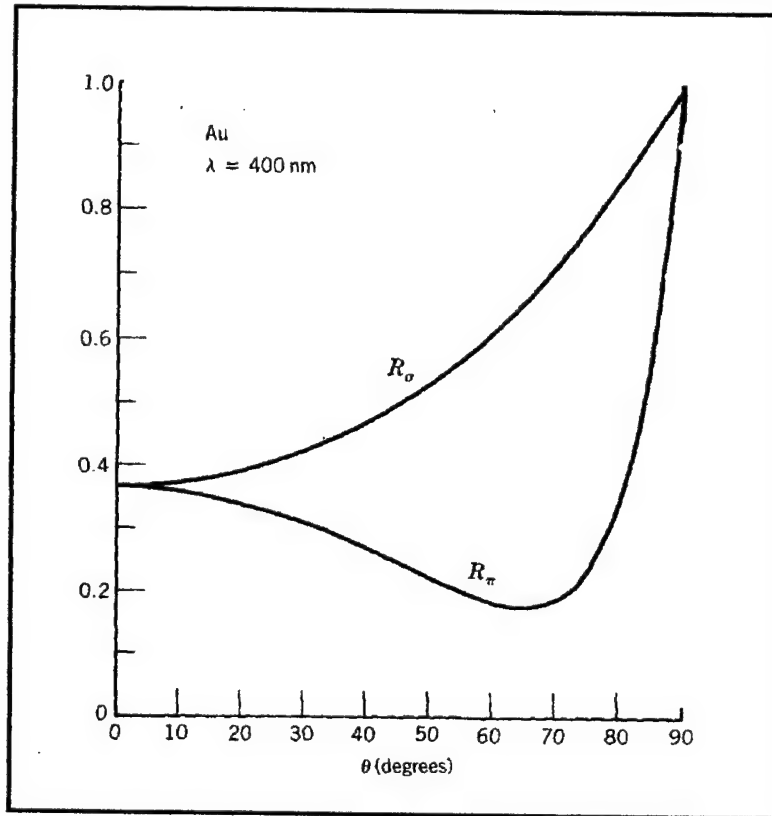


Figure 3.10: Reflectivity of Gold versus Angle of Incidence for Polarized Waves at 400 nm. From Klein (1986).

When Figure 3.10 is compared to Figure 3.8, the variation in reflectance between s- and p- polarized waves is much more significant for the conducting medium. Despite the lack of an angle of zero reflectance, a conducting medium could produce a more distinctive polarimetric difference which could be exploited by remote sensing devices.

4. Selective Absorption

Polarization by absorption results from an interaction of unpolarized light with a medium which preferentially absorbs one polarization component allowing the transverse partner to be either reflected or transmitted. A medium which exhibits this capability is

termed a dichroic polarizer. The dichroic polarizer is physically anisotropic, meaning the properties of the material vary with direction. This characteristic produces a strong asymmetric or preferential absorption of one field component.

An artificial dichroic polarizer consists of a grid of parallel conducting wires. The grid attenuates electric field vectors aligned parallel to the wires due to the currents induced by the field vector arriving normal to the alignment of the wires. Thus light which arrives normal to the alignment of the grid is passed.

There are certain natural materials, however, that are dichroic because of an anisotropy in their crystalline structures. This anisotropy produces a complex index of refraction that depends on crystallographic direction. For these substances there is a principal or optic axis which is defined as a line normal to the incident electric field vectors which are strongly absorbed by material. Tourmaline and herapathite are examples of naturally occurring dichroic materials. (Guenther, 1990, pg. 524)

D. REVIEW OF POLARIZATION DETECTION STUDIES

Polarization has received renewed interest in terms of discriminating targets from background clutter as it provides a level of characterization not available from pure intensity measurements.

1. Polarization Characterization for Target Surfaces

In a paper published in 1995, Nee provided the results of his investigation of polarization characteristics of reflection and near-specular scattering by target surfaces at oblique incidence in both the visible and the infrared. He measured polarization by relatively smooth surfaces for quartz, smooth aluminum mirrors and HfO_2 dielectric film. He investigated rough surface effects on polarization by measuring polarization response for rough quartz and black anodized aluminum samples.

Nee (1995) concluded that reflection from transparent surfaces produced large linear polarization and little circular polarization and that linear polarization for rough transparent surfaces was similar to smooth transparent surfaces. Reflection from metallic

mirrors generated large circular polarization and little linear polarization with larger circular polarization from rougher mirrors. Reflection from dielectric films on semiconductor substrates produced large linear polarization as well as circular polarization.

In a second paper published that same year, Nee and Nee (1995) presented results of their study of linear and circular polarization signatures for targets of known geometric shapes. Using metallic and non-metallic substrates with and without dielectric coating, the generation of reflected and emitted polarization was modeled for flat and cylindrical surfaces.

As a result of their study, they found that dielectric coatings and surface roughness enhance the generation of circular polarization. They concluded that since most target surfaces are rough, the use of circular polarization signatures for target detection and identification would be feasible.

2. Midwave Infrared Polarization

Rogne et al (1995) presented a study which collected background data in order to evaluate the application of passive infrared linear polarimetry for detection of dim air vehicles or ground targets observed against cluttered terrain backgrounds. A high sensitivity midwave infrared polarimetric imager was designed and built based on the use of a MWIR InSb focal-plane camera using a Brewster's angle beamsplitter to separate the vertical and horizontal components. The components in turn were imaged onto different parts of the detector. The imager was sensitive to a spectral band of 4.6 - 4.9 μm with an imaging field of view of 10 mrad. Each image consisted of a 40 x 40 pixel field where each pixel is 1 mrad in extent. Data was collected both in the air and on the ground. Ground collections included imaging samples of target panels, grass, trees and other targets of opportunity including an M-60 tank and an M-35 truck. Air collections of the local Ann Arbor, Michigan area and of Andros Island, Bahamas were made using a helicopter and a twin engine fixed wing aircraft.

In Figure 3.11, three different scenes were sampled with polarimetric imagery. The first column displays an unpolarized image as would be seen by a regular infrared

imager. These images were constructed by combining both vertical and horizontal images from the instrument and use a gray scale which spans the minimum/maximum image radiance. The second column consists of images made from vertically polarized light only. In this case the unpolarized light is removed using data from the horizontally polarized image. The last column shows an image of horizontally polarized light only. The V-H and H-V images are scaled from 0-20 μf ($\mu W/cm^2 \cdot sr \cdot \mu m$), where values less than 0 are set to black and values greater than 20 are set to white. What is important to note in Figure 3.11 is that the tree/sky scene does not exhibit a polarization effect, while the car and the shed roof show strong polarized signatures. This is understandable since the two polarizing objects are constructed with conductive material and, as discussed earlier, this material exhibits selective absorption depending on polarization of the incident radiation.

In another series of images, shown in Figure 3.12, an M-35 truck and an M-60 tank are sampled along with a natural background of grass and trees. Again the grass/tree scene provides very little polarization, while the truck and tank show a strong polarized signature. What is interesting in this series of images is that the fabric on the truck produces a polarized signature, proving that the source of polarization does not necessarily have to be metal in nature.

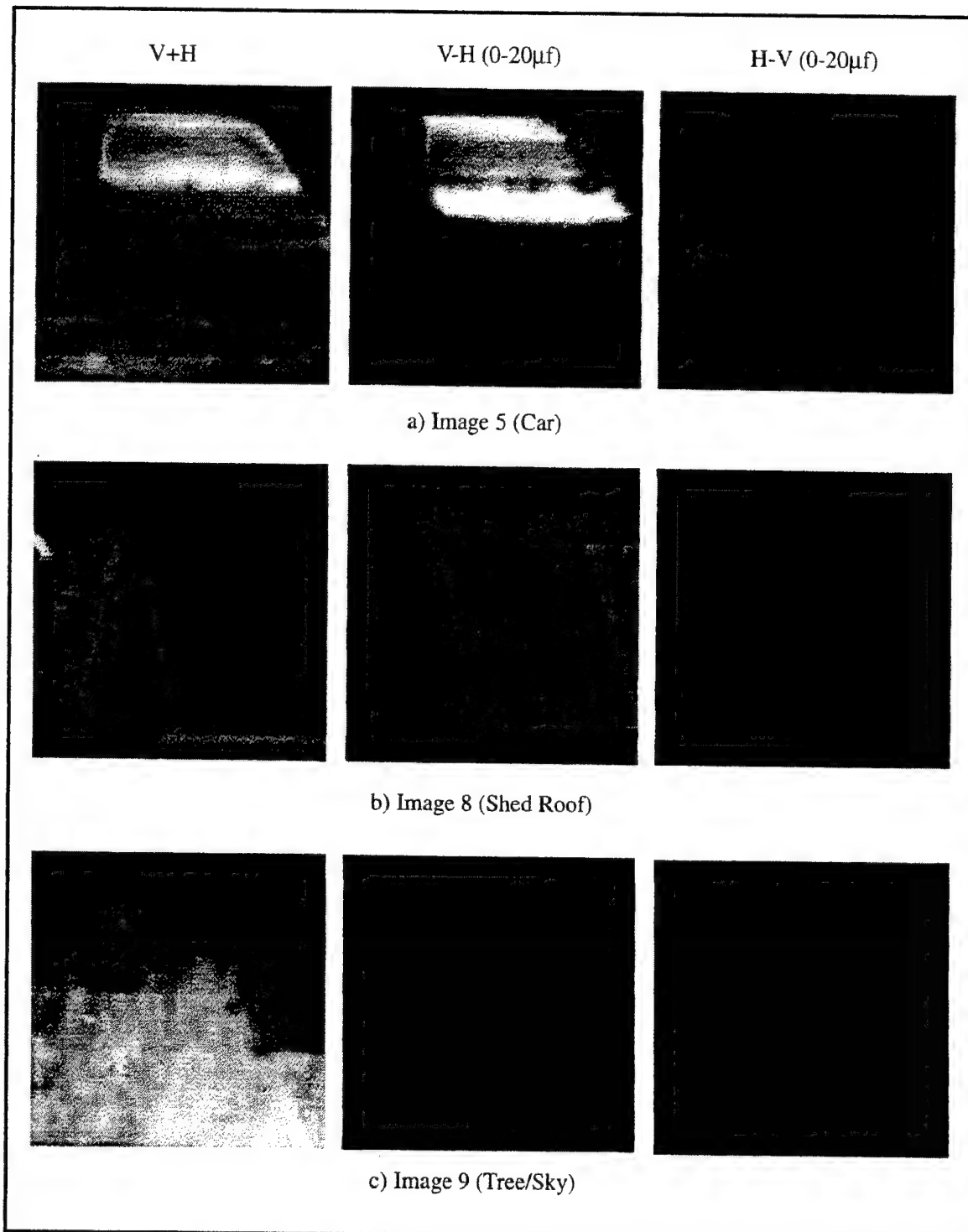


Figure 3.11: Unpolarized, Vertically Polarized and Horizontally Polarized Images of Various Scenes. Rogne et al (1995).

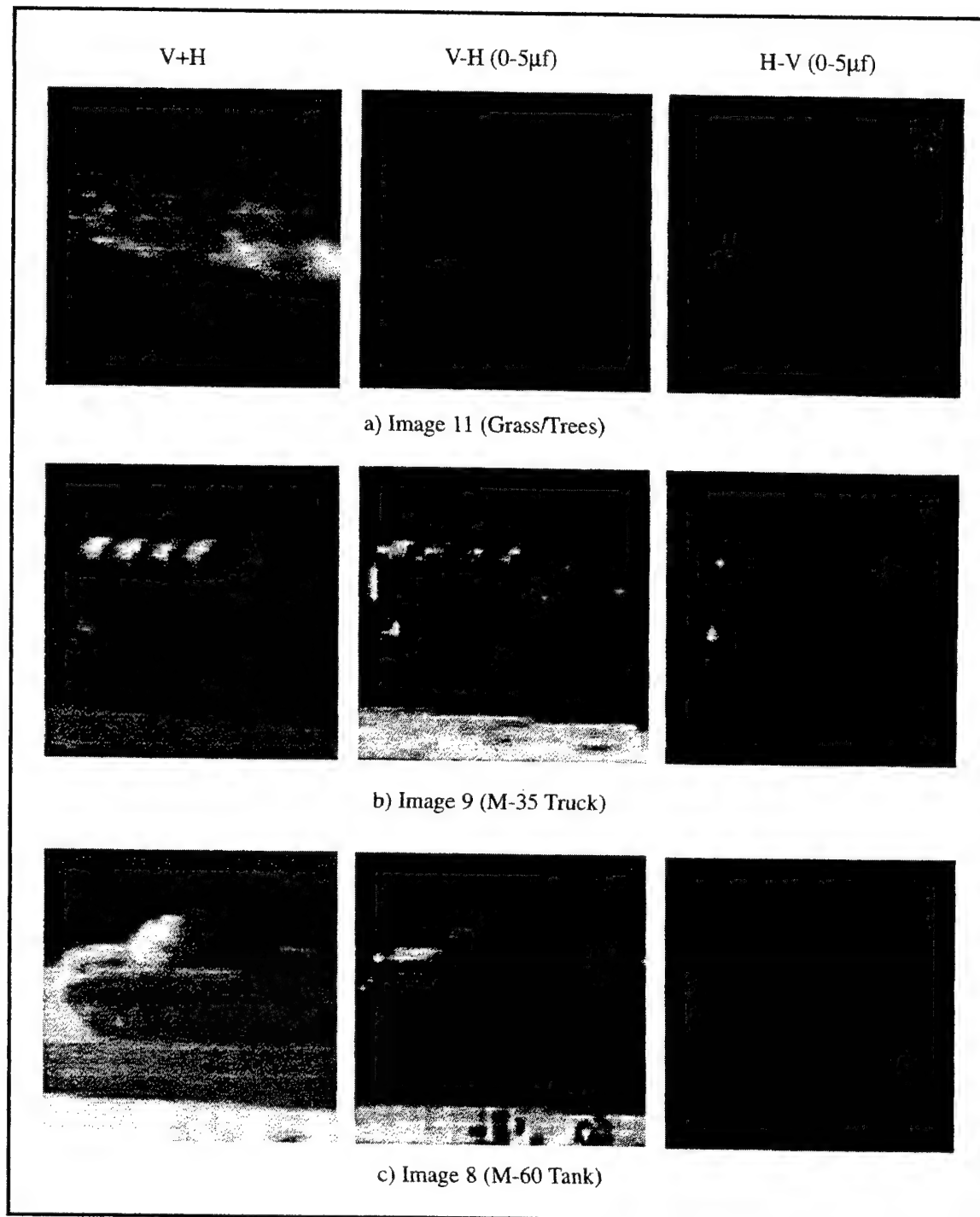


Figure 3.12: Unpolarized, Vertically Polarized and Horizontally Polarized Images of Various Scenes. From Rogne et al (1995).

Figure 3.13 is a scatter plot which compares vertical and horizontal radiance components of several samples including Images 8, 9 and 11 from Figure 3.12. Data

points which fall on the line represent materials featuring low mean polarization. Data points above or below the line represent sources of polarized reflected light. Notice that grass and tree sources are highly correlated and fall along the line of low mean polarization.

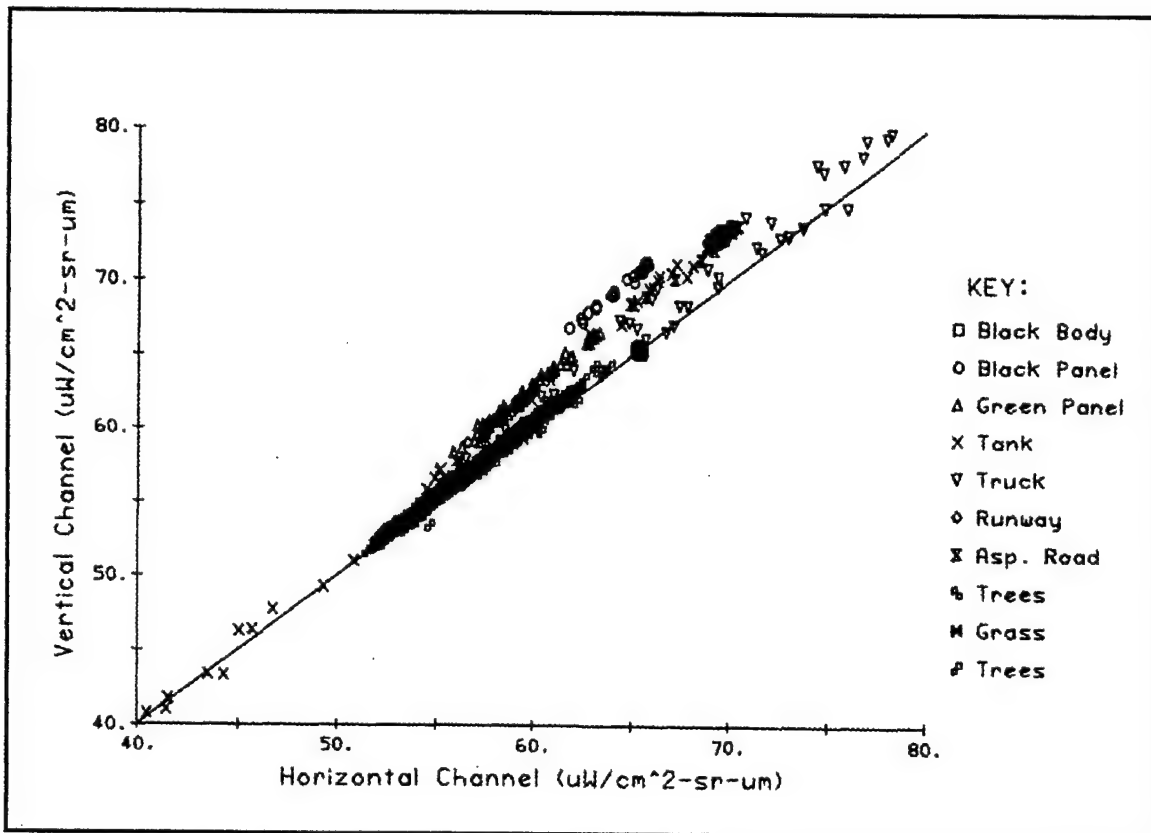


Figure 3.13: Scatter Plots of Selected Signatures. From Rogne et al (1995).

During several collections, the team was able to use a Bomem Fourier Transform Spectrometer in concert with the Imaging Polarimeter in order to compare data. To perform the comparison, two spectral bands centered at $4.629 \mu m$ and $4.855 \mu m$ were selected from the measured data. These bands were chosen as they exhibited the maximum difference in color within the $4.6 - 4.9 \mu m$ band observed by the polarimetric imager. Table 3.1 provides the observed data from one such collection. The value of SCR_{H+V} represents the signal-to-clutter ratio of an unpolarized radiometer, while $SCR_{H,V}$ represents signal-to-clutter for a polarized radiometer. This allows a comparison of

single pixel target detection performance between unpolarized single channel data and polarized two channel data. The improvement in detectability is listed as Gain. For the FTS data, SCR_1 represents single channel data using the best of the two channels. This would be comparable to the unpolarized radiometric data. SCR_2 represents the signal-to-clutter ratio when two bands are used for detection.

Table 3.1: Comparison of Detection Performance for MWIR Polarimeter and Fourier Transform Spectrometer. From Rogne et al (1995).

Case	Polarimeter (dB)			FTS (dB)		
	SCR_{H+V}	$SCR_{H,V}$	Gain	SCR_1	SCR_2	Gain
Black Panel, Grass	19.1	29.2	10.1	11.4	18.4	7.0
CARC Green, Grass	0.5	23.2	22.7	4.7	19.2	14.5
Tank, Grass	19.1	24.8	5.7	10.0	22.6	12.6
Truck, Grass	3.1	16.5	13.4	0.5	19.3	18.8
Black Panel, Trees	13.2	26.6	13.4	16.2	20.2	4.0
CARC Green, Trees	6.2	20.8	14.6	-9.0	16.4	25.4
Tank, Trees	13.2	22.0	8.8	6.4	19.7	13.3
Truck, Trees	6.7	15.0	8.3	9.7	18.6	8.9

From their study, Rogne et al arrived at several key results. They found that rural clutter (vegetated scenes) exhibits low mean degrees-of-polarization. The vertical and horizontal polarized channel responses to rural clutter are very highly correlated resulting in large clutter suppression and therefore high detectability of polarized targets. They found that while water is a key polarized clutter feature (typically 1-3% mean degree-of-polarization), water clutter is highly correlated leading to good clutter suppression and enhanced detectability for polarized targets. Small patches of water, however, are a potential problem for false alarms. Limited ground based measurements indicated little or no mean polarization and high correlation for sky and cloud clutter. Their study also showed that painted aircraft surfaces observed at altitude exhibit a strong polarization signature.

Rogne et al (1995) concluded that polarimetric sensing could significantly enhance the detectability of low radiometric contrast targets in rural clutter. They found that the mean degree of polarization for most natural backgrounds is below 0.2% and that clutter correlations between vertically and horizontally polarized light is very high, often exceeding 0.99. Additionally, they suggest that spatial filtering could be used to enhance target detectability within polarimetric data.

3. Polarimetric Analysis of Hyperspectral Data in the Visible Spectrum

Sturgeon (1993) conducted an analysis of data collected during a ground based experiment using an acousto-optic tunable filter (AOTF) hyperspectral imaging system to illustrate the utility of hyperspectral imagery for military applications. The instrument collected vertically and horizontally polarized images in 33 spectral bands between 0.51 and 0.77 μm . In conjunction with an analysis of hyperspectral target detection, a polarimetric study was conducted.

The first imaged scene that was analyzed contained a communications site with four separate camouflaged pieces of equipment in a desert background. Camouflage included dark green and woodland types. A comparison of the spectral curves for the camouflage nets at each polarization produced a relatively large difference at 0.58 μm . The next scene also contained a communications site in the desert, but the equipment was concealed under desert or tan camouflage nets. Again there were discernible differences in polarimetric response as was experienced in the third scene which contained military equipment under woodland camouflage in a stand of trees.

Sturgeon concluded that while polarimetric analysis of the AOTF data provided information about the polarimetric characteristics of surface features, the contribution to detection of camouflage was not significant. However, the data available to Sturgeon was limited to a rather narrow wavelength range. As seen in the MWIR study by Rogne's team, there is data available throughout the spectrum.

IV. PROPOSED APPLICATION OF POLARIMETRIC DATA TO HYPERSPECTRAL IMAGERY ANALYSIS

This chapter presents a proposed method for analyzing hypercube data which exploits polarization characteristics of targets. Additionally, the second section of the chapter outlines two proposed experiments designed to understand the possible impact polarization can have in hyperspectral data analysis. The first experiment is designed to investigate polarization variation throughout the spectrum and ascertain whether there exists detectable characterizations for polarization difference. The second proposed experiment will leverage off results from the first and attempt to validate the polarization filtering techniques just described.

A. DESCRIPTION OF ANALYSIS TECHNIQUE

From previous studies, it was shown that polarized light is produced by many objects, but that vegetated backgrounds produce little to no polarization (Rogne et al, 1995 and Sturgeon, 1993). This characteristic makes target detection possible in a vegetated scene due to the polarimetric contrast. Additionally, the degree of polarization may be wavelength dependent and therefore the difference of intensity between s- and p-polarized light may also demonstrate a wavelength dependence.

As mentioned in the discussion of hyperspectral imagery analysis, the amount of data in a hypercube is enormous compared to a panchromatic image. This requires dealing with data storage and transfer issues, which can be a real problem particularly for a sensor carried onboard a satellite similar to the one proposed in the Warfighter 1 Program. Additionally, the use of hyperspectral imagery in a tactical environment requires rapid analysis of data with rapid dissemination of information to the warfighter. It is in this tactical realm that polarimetric data may be of the most value. Past studies have dealt with the concept of characterization of a target by polarization. While this may be of use, the time for analysis of the imagery will be greater since there are now

two hypercubes of data which have to be analyzed. Here we propose a more modest use of polarimetric characterization for simplifying the analysis of the hypercube.

This proposed analysis technique seeks to exploit two phenomena. First is, of course, a strong polarimetric response by the target in comparison to the background. Second, that the intensity of polarizations created by the target varies with wavelength such that there is a particular wavelength or wavelengths where a maximum difference in intensity exists as shown in Figure 4.1. Likewise it is important to know at what wavelength the minimum difference occurs. For demonstration purposes, PD_{MAX} and PD_{MIN} will be used to represent these wavelengths.

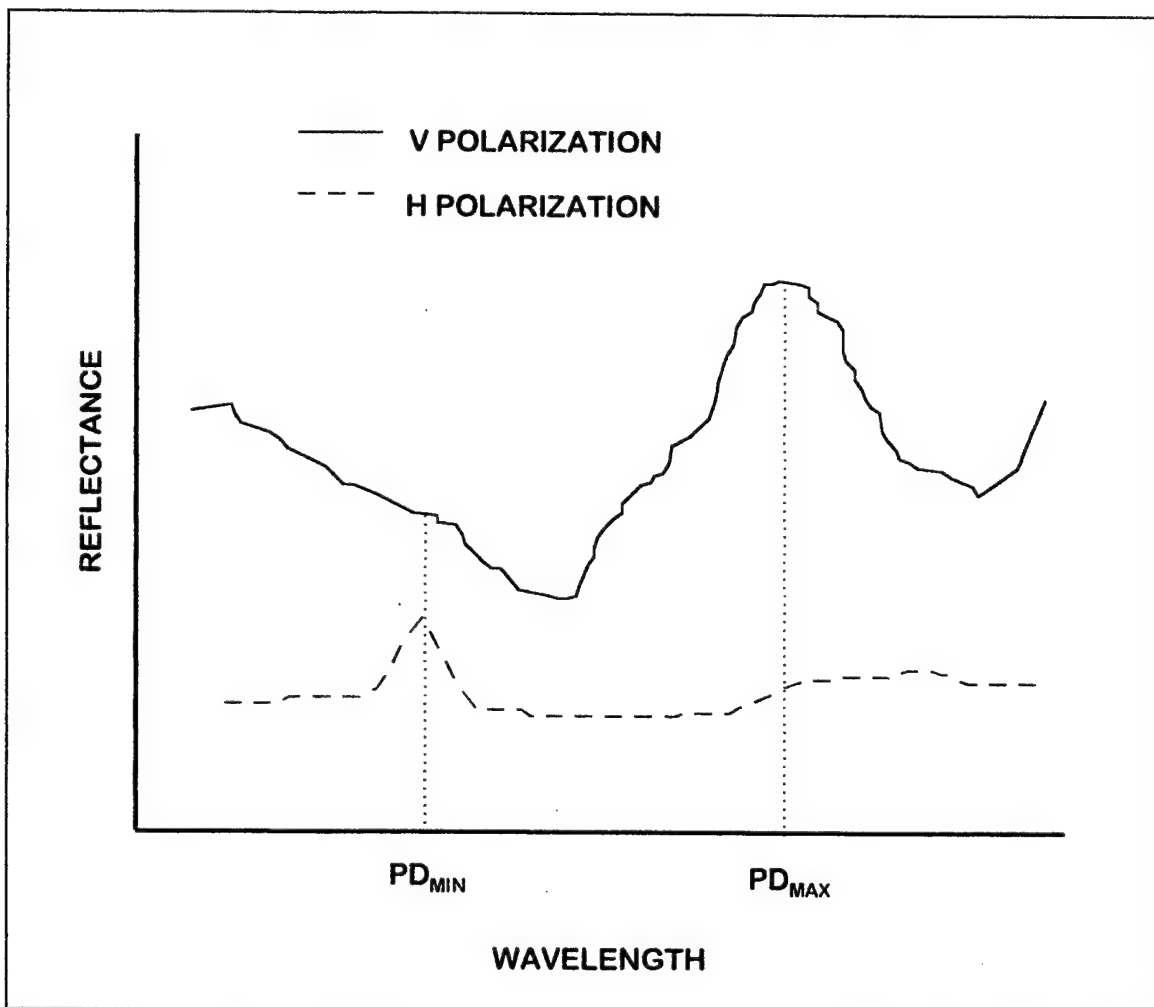


Figure 4.1: Spectrum of Vertical and Horizontal Polarizations for a Hypothetical Material.

Assume that a hyperspectral imager is modified to collect two polarized hypercubes of data, one for vertically polarized light and one for horizontally polarized light. We are interested in detecting a target with the polarization reflectance curve depicted in Figure 4.1. Two hypercubes are collected of a scene with numerous objects. Knowing PD_{MAX} for the target, we extract the V and H images from the two hypercubes at the wavelength corresponding to PD_{MAX} and compare the scenes using a correlation program. Objects exhibiting high correlation, such as would be the case for trees, are removed. As shown in Figure 4.2, any differences between the two images indicates the presence of polarizing objects, among which may be the target of interest.

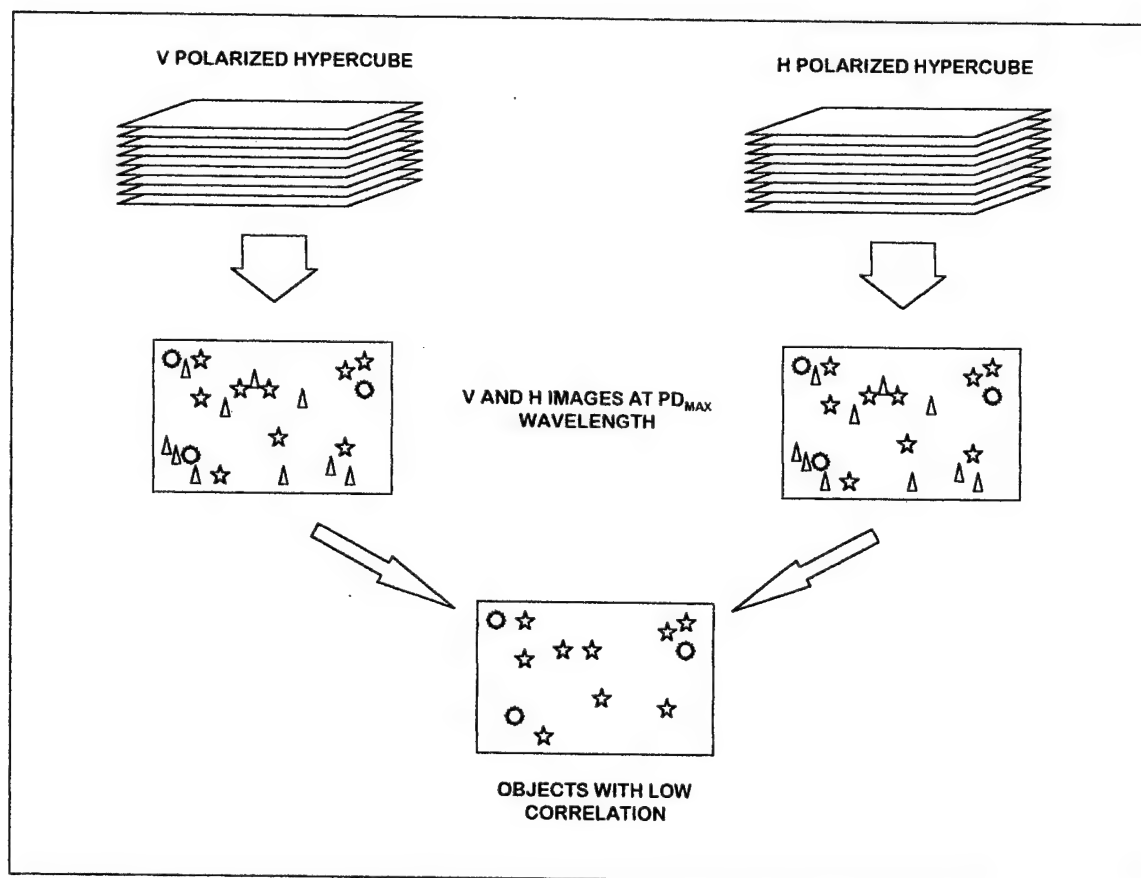


Figure 4.2: Polarimetric Filtering Technique for Hypercube Data.

We have now successfully reduced the number of pixels which require analysis. At this point it is possible to extract spectral data at each of the pixels of interest and continue with traditional hyperspectral analysis to differentiate the target from other

objects which exhibit polarization at PD_{MAX} . However, there may be a large number of different objects within the scene which exhibit polarization at PD_{MAX} . A second stage of filtering could be applied in order to reduce the number of false alarms. Many objects, such as water, exhibit fairly strong polarization throughout the entire spectrum and could easily become a source for false alarms at any wavelength. If the target object exhibits a reduced polarization intensity difference, such as exists at PD_{MIN} from Figure 3.13, this characteristic could be exploited in a similar manner as the first technique. As shown in Figure 4.3, V- and H-polarized images from both PD_{MAX} and PD_{MIN} are extracted from the two hypercubes and compared for correlations. The two resulting images are then compared for correlation. Objects exhibiting high correlation are once again removed, as they represent objects which still exhibit strong polarimetric intensity differences. This leaves us with an image of all objects exhibiting the PD_{MAX} and PD_{MIN} of the target of interest.

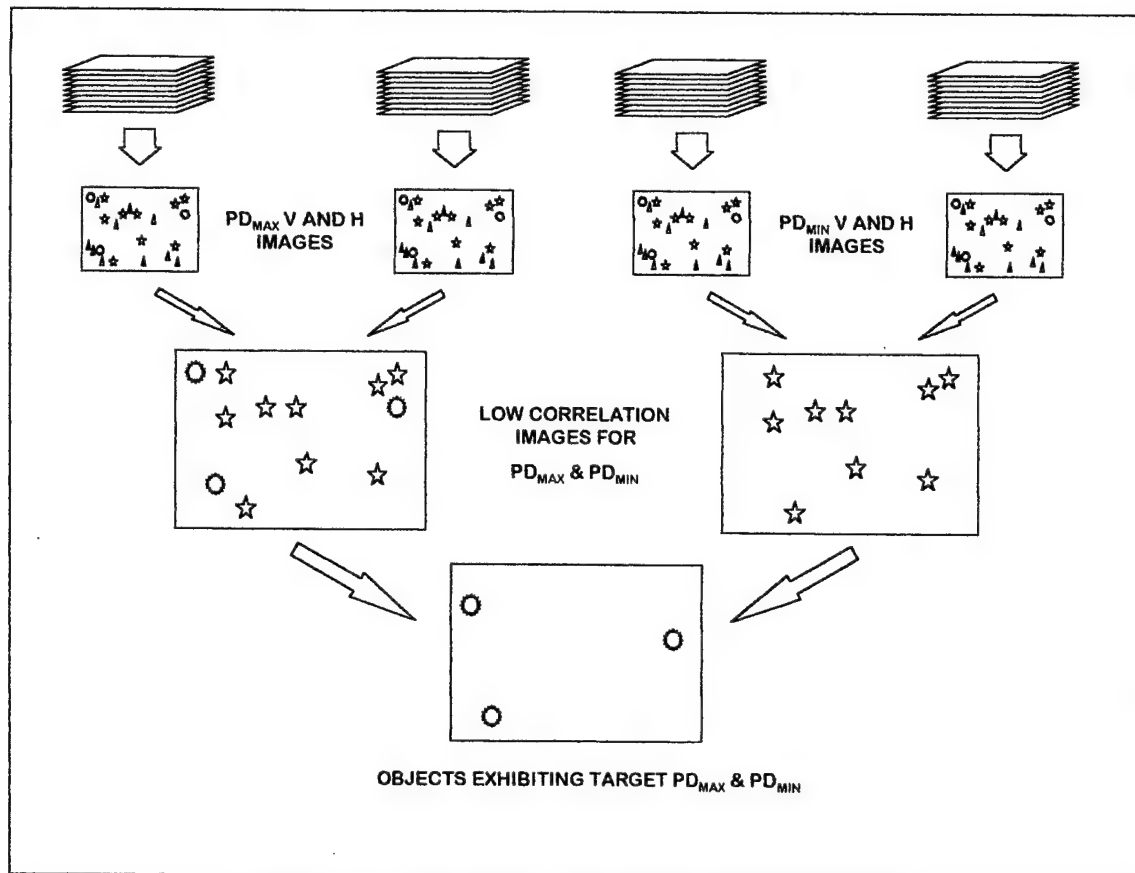


Figure 4.3: Two-step Polarimetric Filtering Technique.

At this point we have reduced the number of pixels containing possible targets. The hypercubes can now be analyzed using traditional hyperspectral techniques at those pixel locations. Since we have reduced the number of pixels in question, the time for data analysis has been significantly reduced.

This technique poses several problems, however. Perhaps the most important is the need for at least two hypercubes of data. This will require twice the storage capacity that a traditional hyperspectral imager would require. Second, the instrument would necessarily be more complex and perhaps larger. Additionally, calibration of two data sets is now required. If separate imagers are used to collect data, the calibration problem is even more complicated. Careful consideration of the method of separating V and H polarizations would be required to minimize signal loss. Accurate pixel-to-pixel channel registration is crucial for accurate image correlation.

Benefits of this technique, however, are numerous. What this technique suffers in data storage requirements, it makes up for in data transfer. If the sensor platform also carries limited data processing equipment to conduct polarimetric filtering, only the spectral data for the pixels of interest need be transmitted. Additionally, since we are only concerned with polarimetric differences, atmospheric compensation, and that entire data massaging process, is obviated until after the possible target bearing pixels are selected and actual spectral analysis begins.

Several assumptions were made in developing this technique. While some studies have indicated wavelength dependence for polarimetric intensity differences, they do not specifically address this phenomenon and the data is limited. Second, the enhancement of reduced data analysis time is merely speculation and requires research. Time gained in reducing the number of pixels which require full spectral analysis may be in exchange for time lost in data collection and registration. Finally, the most impressive results to date use panchromatic imagery in the midwave infrared. The effectiveness of polarimetric characterization in the visible to shortwave infrared should be examined.

B. EXPERIMENT DESIGN

1. Spectral Variation of Polarization

The purpose of this experiment is to measure radiometrically the polarization characteristics of certain objects of military interest to include various backgrounds. Reflectance samples of various objects are collected for both vertical and horizontal polarizations and then analyzed to determine if any significant characteristics exist. Maximum and minimum reflectance difference will be computed between the two polarized spectral reflectance curves.

a. Instrumentation

The proposed instrument for this collection is the FieldSpec Portable Spectroradiometer manufactured by Analytical Spectral Devices, Inc. of Boulder, Colorado. The particular model desired is the FieldSpec UV/VNIR. As shown in Figure

4.4, this unit contains a built-in sub notebook with an enhanced parallel port for the Spectrometer Computer Interface. A 1.2 meter fiber optic cable provides light sample input to the spectroradiometer with a 25° full angle cone of acceptance field of view. The fiber optic cable can be plugged into one of a number of field of view fore optics, shown in Figure 4.5, for use in longer range detection or when a smaller field of view is desired. The unit weighs 5.4 kg and the additional battery pack adds 2 kg. (Analytical Spectral Devices, Inc., 1995)

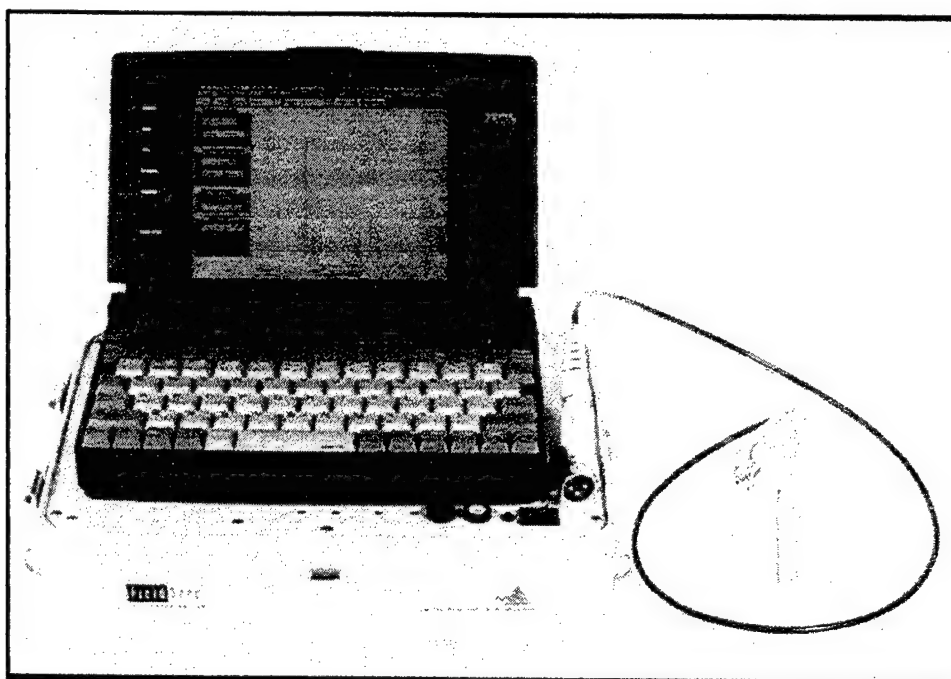


Figure 4.4: FieldSpec Portable Spectroradiometer with Fiber Optic Collector. From Analytical Spectral Devices, Inc. (1995).

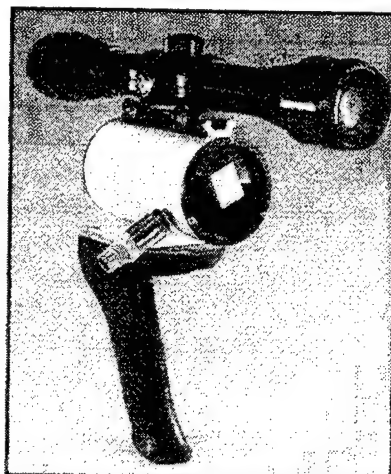


Figure 4.5: Mirror Fore Optic. From Analytical Spectral Devices, Inc. (1995).

The sensor consists of a 512 element low dark current NMOS photodiode array which operates at room temperature. A fixed concave holographic reflective grating is used for spectral dispersion. Spectral range of the instrument is 0.35 to 1.05 μm with a spectral resolution of 3 nm and wavelength accuracy of ± 1 nm. A 5 x 5 inch white Spectralon panel is used for reflectance calibration. Full 0.35 - 1.05 μm raw Digital Number (DN) or reflectance spectrum is displayed in real-time by the sub notebook computer. Data storage for each sampled spectrum requires 2.5 KB of hard drive space. The computer is based on a 486DX-100 microprocessor and contains a 3.5" floppy drive and a 300 MB hard drive. (Analytical Spectral Devices, Inc., 1995)

The orientation of reflected polarized light should be selectively sampled by use of a dichroic sheet polarizer. This type of polarizer is composed of polymeric plastic which is stretched and sandwiched between strain-free glass plates. By stretching the plastic, the molecules in the material are oriented in a particular fashion. The selective addition of pigments to the stressed polymer permits preferential absorption of one polarization due to the orientation of chemical bonds. The plane of preferred transmittance is marked by engravings on the ring in which the polarizer is mounted. This device will be attached to the fore optic of the spectroradiometer and ring will be rotated to alter the angle of polarization. (Melles Griot, 1990, pp. 14.22 - 14.23)

b. Data Collection

As shown earlier by Rogne's study, vegetated background tends to reflect unpolarized light while other objects, such as metal roofs, cars and trucks, reflect polarized light. Differentiating between objects and the background would therefore be the first object of this investigation. For the two step polarization filtering method to be useful, differentiation between targets and non-targets would be required. With this in mind, the data collection strategy for polarization spectra should include targets, non-targets and background. The subjects of collection in the target category should represent military equipment such as tanks, heavy trucks, aircraft, camouflage nettings, buried mines, and any other military related hardware. The subjects of collection in the background category should include soil, rock, trees, brush, grasses, water, roads and other non-target related objects which would be present in a scene. The subjects of collection in the non-target category are harder to list but would generally consist of objects which produce strong polarization, but are not targets. The intent is to understand the polarimetric characteristics of all objects in a scene to allow investigation into what polarimetry can and can not do.

Calibration of the instrument in the field is a fairly simple process. Prior to a sampling session, the probe is directed at a white reference card and the WR (white reference) on-screen button is depressed. This measurement is stored as a baseline for automatic real-time calculation of target reflectance measurements. During the calibration measurement the software adjusts the gain for optimal performance and instrument offsets are measured and stored for automatic subtraction from reflectance calculations. Periodically, it is necessary to make offset correction measurements. The DC on-screen button is depressed and the instrument automatically records offset using a built in shutter system. Offset data is automatically subtracted from target and white reference data. (Analytical Spectral Devices, Inc., 1995)

While the system is calibrated for the installed optics, it does not compensate for the dichroic polarizer. Unfortunately, the optical density of the polarizer varies with wavelength. If the difference in optical density remained constant between the open and closed positions throughout the spectrum, no correction would be required

as we are only concerned with intensity differences. As shown in Figure 4.6, however, this is not the case and some correction must be made.

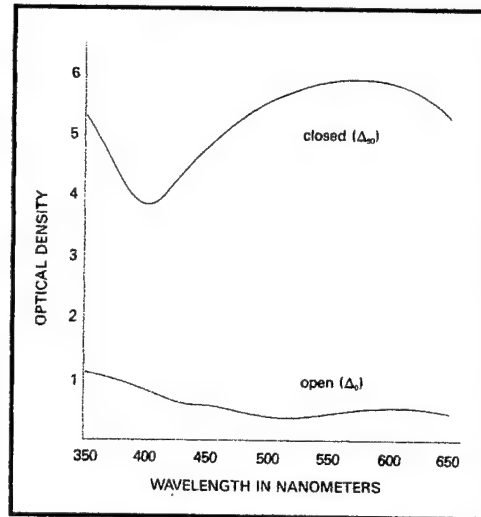


Figure 4.6: Optical density Variation of a Dichroic Polarizer. From Melles Griot (1995).

One method to compensate for this variation is to calibrate the system using artificial light to ensure consistent irradiance. The white reference card is sampled as it would for a normal calibration but with the polarizer out of the optical path. The polarizer is then installed and the white reference card is sampled again. The resulting reflectance curve could be downloaded and applied to sampled data to correct for non-linearity of optical density through the spectrum.

Actual sampling of objects should be accomplished using a tripod mount or some other form of stabilization in order to fix the position of the sensor while measuring both vertical and horizontal polarized spectra. Various geometries based on sun arrival angle should be considered based on Brewster's angle phenomena and other anomalies. Since the FieldSpec Spectrometer can provide real-time measurements, every attempt should be made to orient the polarizer to achieve maximum reflectance values. Once achieved, a sample is taken and stored, the polarizer is then rotated 90° and a second sample is taken for minimum polarization intensity.

c. Data Analysis

The FieldSpec Spectrometer stores samples in binary form and is capable of exporting files in ASCII and other file types. Data analysis may be accomplished using simple programs written in IDL or even spreadsheet programs. Data consists of reflectance measurements which are calculated in a manner similar to Equation (2.4) as

$$\rho(\lambda) = \frac{\text{offset - corrected raw DN reflected from target}}{\text{offset - corrected raw DN reflected from white reference}} \quad (4.1)$$

where raw DN is the digital number from the detector-Analog/Digital system. Thus the reflectance values are effectively corrected for solar irradiance variations as well as atmospheric absorption. The first step in the data analysis is to correct for optical density variations in the polarizer. Next, the difference in reflectance values between V- and H-polarizations for each sampled spectral band is calculated and plotted against wavelength. Finally, the points of maximum and minimum intensity differences and their associated wavelengths are computed and printed out. From this information, PD_{MAX} and PD_{MIN} are known and can be incorporated into the polarization filtering algorithm.

2. Polarized Hyperspectral Imagery

The use of an actual hyperspectral imager would obviate the need to conduct the first experiment. If the object imaged in the scene were known, a pixel of hypercube data from that object's image could be extracted and the reflectance spectra could be analyzed using the algorithm explained in the first experiment. This technique would provide essentially the same results. Unfortunately, hyperspectral imagers are costly devices and limited in availability, therefore alternate methods must be used to validate the two step polarization filtering concept.

This experiment makes use of a standard digital camera in lieu of a hyperspectral imager. Using the maximum and minimum wavelengths found for various objects and backgrounds in the first experiment, narrow spectral width bandpass filters are used in

conjunction with the dichroic polarizer to image a scene. The data is then analyzed using the two step polarization filtering process.

a. Instrumentation

A rather primitive polarimetric hyperspectral imager would consist of a Canon EOS DCS 1 digital single lens reflex camera, selected filters and a polarizer. The camera, as shown in Figure 4.7, is based on Canon's EOS-1 camera body and is compatible with all Canon EF series lenses. The viewfinder uses an eye-level reflex pentaprism with a frame to indicate the portion of the image to be captured by the focal plane array. The array itself measures 27.6 x 18.4 mm (3060 x 2036 pixels) with an individual pixel size of 9 x 9 μm providing over 6 million pixels of data. The camera uses 12 bit digitization and each image requires 6MB of storage which is handled by a removable PCMCIA-ATA hard disk card. A 170 MB hard disk can store up to 26 images.



Figure 4.7: Canon Single Lens Reflex Digital Camera. From Canon (1996).

To sample the correct wavelength requires the use of bandpass filters, in this case, interference filters. As shown in Figure 4.8, narrowband interference filters permit isolation of wavelength bands down to a few nanometers without the use of dispersion elements. They are typically multilayer thin-film devices which make use of the same principles employed by Fabry-Perot interferometers. Each filter is mounted in a black anodized aluminum ring. While this arrangement only captures one single spectral band image at a time, it has enormous throughput advantage compared to hyperspectral imagers which are required to reduce the image to a slit to enable the dispersion technique. Finally the dichroic sheet polarizer comes into play once again in the same manner as was used in the first experiment.

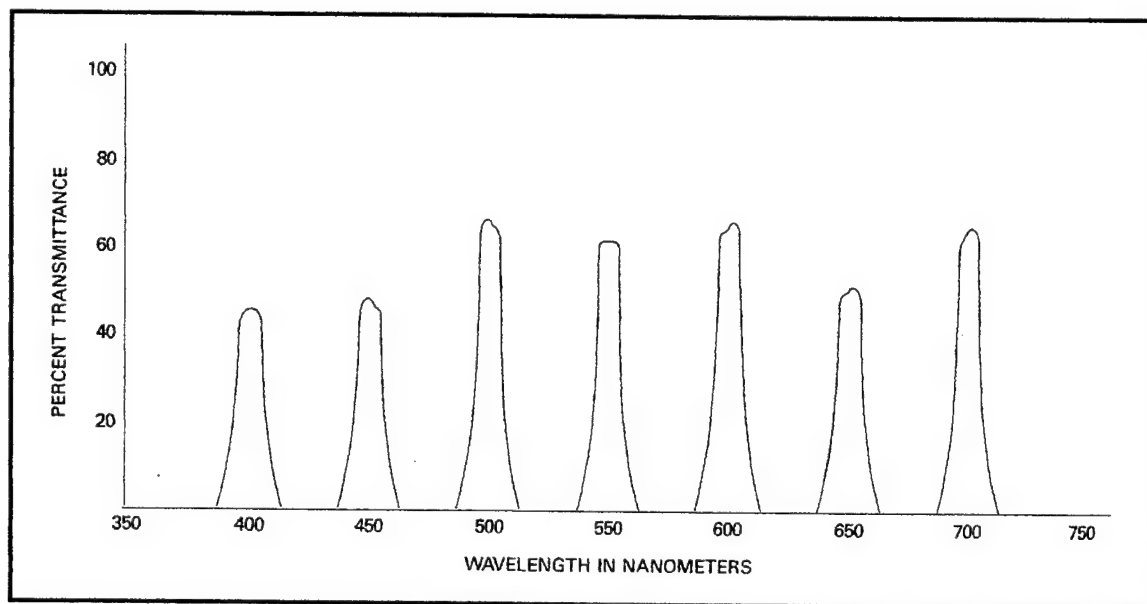


Figure 4.8: Wavelength Bandpass for Various 10 nm Interference Filters. From Melles Griot (1990).

b. Data Collection

Unlike the first experiment where spectra of single objects were collected individually, we are collecting an image of a scene which requires a much larger field of view. To accomplish this, however, requires the sensor to be elevated which creates

some logistical difficulties. Due to the time interval required for changing polarizer orientation between samples, a moving platform, such as an aircraft or helicopter, would create significant image registration problems. Booms could be employed, but unless they were man-lift type, they would require that the instrument be lowered to facilitate changing the polarizer orientation. Alternatives such as rooftop or tower collections should be explored. The use of low angle collection such as imaging across a field from near ground level may provide interesting data, but does not adequately simulate an overhead remote sensor.

The data collection strategy should look to initially minimize the number of polarization sources in the scene. For instance, a grass field containing some trees and a tank would provide a rather uncomplicated scene in the polarization sense. Gradually more complicated scenes should be imaged depending on the results from previous collections. It would be important to collect an image that has water somewhere in the scene, since water is a strong polarizing source. This sample would permit a good test of the two step polarization filtering technique. As in the previous experiment, the camera should be mounted or stabilized to fix its position between the two polarization images. Additionally, varying sun angles should be accommodated during the collections. Consideration should be given to concurrently sampling objects in the scene using the field spectrometer in order to verify existence of polarization differences for that collection. In this case, use of the high power fore optics would allow sampling from the same platform used by the camera, reducing geometrical variance.

Calibration of the camera's response is a bit more problematic than the field spectrometer. Since the most critical measurement relates to determining the wavelength for maximum and minimum polarization difference, which was conducted in the first experiment, calibration of the camera is perhaps unnecessary. Variability across the focal plane array may have a limited effect, but this can be compensated for during post-collection data analysis by borrowing the white reflectance panel from the field spectrometer and imaging the panel. Pixel-to-pixel variation can then be compensated by taking the mean brightness observed by the array, determining variation from the mean

pixel by pixel and adjusting data for each pixel variation. This is perhaps a bit extreme for the level of this experiment and it is recommended that pixel variation be ignored.

c. Data Analysis

Image data can be downloaded using provided software which will allow display and translation in other file types. Analysis of this data requires an IDL program which processes the data per the algorithm shown in Figure 4.9. It is very important that the V- and H-polarized images are registered pixel by pixel for proper results. After the possible targets are located image registration to the hypercube is required prior to extracting spectra.

Due to constraints on time and research funds, the experiments described above were not conducted as part of this thesis, but will be conducted in follow-on work.

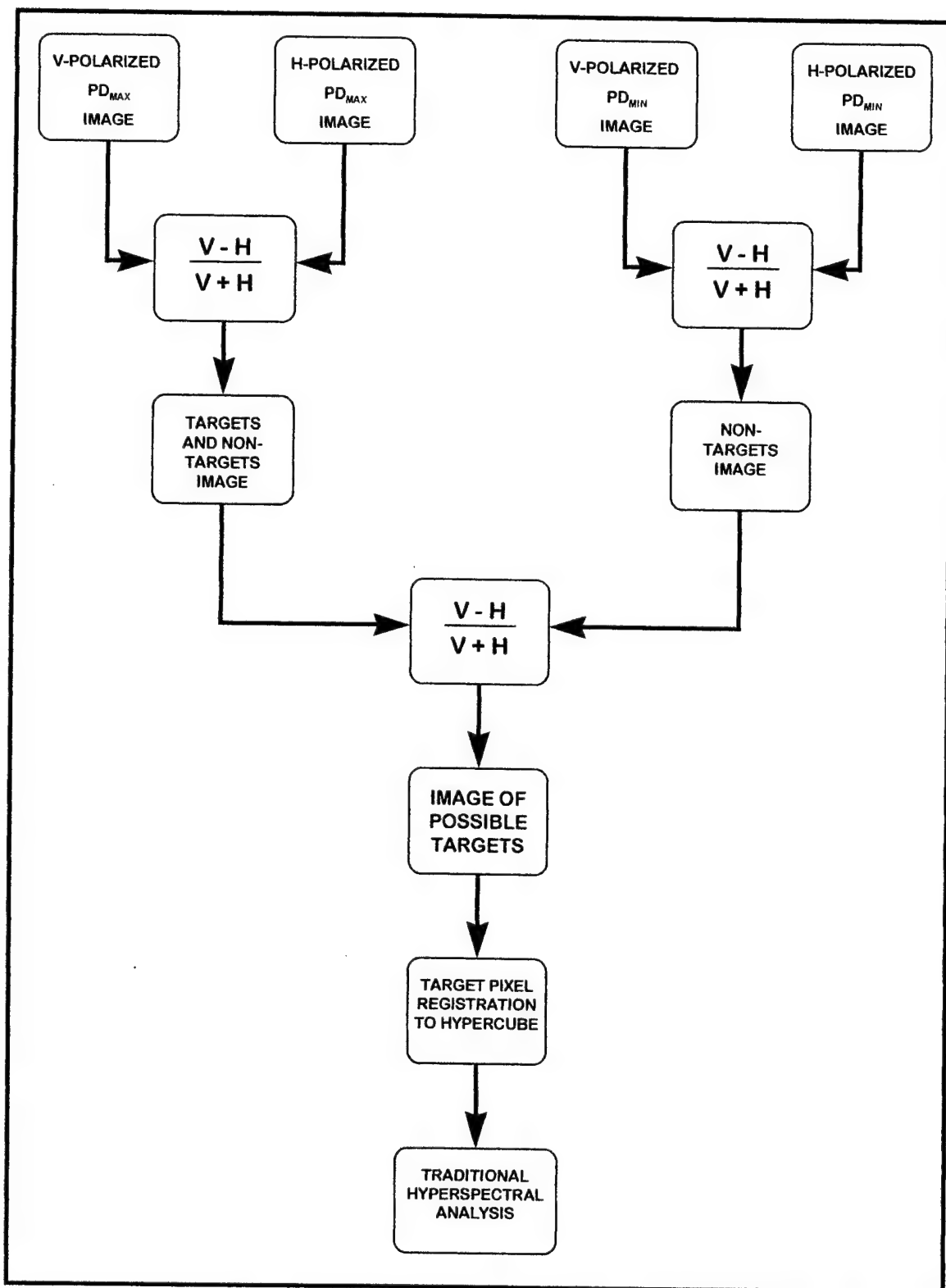


Figure 4.9: Data Processing Algorithm.

V. SUMMARY AND RECOMMENDATIONS

A. SUMMARY

The fundamentals of remote sensing were presented culminating in a discussion on the purpose and theory behind hyperspectral imagery. A variety of hyperspectral sensors, either built or in the process of design, were presented. An analysis of one such system, the proposed Warfighter-1, described the difficulties inherent in the tactical application of hyperspectral imagery and recommended the use of polarimetric data for analysis. Basic polarization theory and fundamentals were presented and a review of recent studies in the application of polarimetric data to target detection was discussed. A hyperspectral data analysis scheme was proposed using polarimetric data and two mutually supporting experiments were proposed to validate the technique. Despite the lack of data, several interesting items were found during the course of research into the idea of using polarization difference characterization for hyperspectral data analysis.

Materials will produce polarized light to varying degrees and various orientations depending on the composition of the material. While not well sampled, there are indications from past experiments that spectral reflectance values from different polarizations vary as a function of wavelength and that there points along the spectrum where the difference between polarizations produce maximum and minimum values. This point is key to the functionality of the two step polarization filter technique. Additionally, polarized light in the midwave infrared provides a strong signature difference between vertical and horizontal orientations for target objects while very little polarization is observed from vegetation and other forms of background. When compared to conventional imaging spectrometers, detectability of certain targets is slightly improved.

B. RECOMMENDATIONS

Continued research to collect spectral polarization characterizations for targets and backgrounds is strongly recommended. To assist in the process, the proposed FieldSpec UV/VNIR Portable Spectrometer should be upgraded, when funding is available, to include the shortwave infrared region out to 2.5 μm . This would allow sampling in the entire band proposed for use by the Warfighter-1 Hyperspectral Imager, as well as provide a larger data set for characterization analysis.

While constructing a polarimetric hyperspectral imager is a daunting and expensive task, it would certainly provide improved data compared to the proposed digital camera experiment. Additionally, the two step polarimetric filtering technique could be applied to an actual hypercube of data rather than preselected images. Short of this, an unpolarized hyperspectral sensor could be used in a similar manner as the digital camera by taking two successive images while rotating the polarization plane of the filter, however pixel to pixel registration problems will have to be addressed.

The two step polarization filter technique is a basic concept intended to evaluate the applicability of polarization to target detection. Further development of the algorithm to include all required corrections and compensations should prove challenging. Other more rigorous analytical algorithms that would provide better results using polarimetric data should be investigated.

While not discussed specifically, it is apparent through this research that certain materials provide very strong polarimetric response to incident light. It may be possible to apply this concept for use in special operations where covert marking of targets for later hyperspectral identification is conducted. Additionally applications of this signature material could be employed in combat search and rescue operations to locate a downed airman or optical IFF systems. Further research in this area is certainly warranted.

LIST OF REFERENCES

Analytical Spectral Devices, Inc., "Analytical Spectral Devices Technical Guide", Boulder, Colorado, (1995).

Anderson, R., W. Malila, R. Maxwell, L. Reed, "Military Utility of Multispectral and Hyperspectral Sensors", Infrared Information Analysis Center, Environmental Research Institute of Michigan, Ann Arbor, Michigan, (1994).

Canon, "EOS DCS 1", Product Information Guide, (1996).

Collins, B. H., "Thermal Imagery Spectral Analysis", Master's Thesis, Naval Postgraduate School, Monterey, California, (1996).

Demro, J. C., and L. M. Woody, "Flight Demonstration of the Wedge Imaging Spectrometer," Tactical Technologies and Wide-area Surveillance International Symposium Proceedings, Counterdrug Technology Assessment Center, (1993).

Department of Defense, "Multispectral Users Guide", U.S. Government, (1995).

Fay, M. E., "An Analysis of Hyperspectral Imagery Data Collected During Operation Desert Radiance", Master's Thesis, Naval Postgraduate School, Monterey, California, (1995).

Guenther, R. D., Modern Optics, John Wiley & Sons, New York, (1990).

Hackwell, J. A., D. W. Warren, R. P. Bongiovi, S. J. Hansel, T. L. Hayhurst, D. J. Mabry, M. G. Mabry, M. G. Sivjee, J. W. Skinner, "LWIR/MWIR Imaging Hyperspectral Sensor for Airborne and Ground-Based Remote Sensing", The Aerospace Corporation, Los Angeles, California, (1996).

Hecht, E., Optics, 2nd edition, Addison-Wesley Publishing Company, New York, (1989).

HRIS Program Office, "Hyperspectral Infrared Imaging Spectrometer Research Instrument System Requirements Review", Briefing Handout, (1996).

HYMSMO Program Office, "Hyperspectral MASINT Support to Military Operations - Achieving Force Multiplier Support to the War Fighters through Nontraditional MASINT Applications", Briefing Handout, (1993).

Integrated Space Technology Demonstration Program Office, "Warfighter 1 Statement of Objectives", Version 1, ISTD Program Office, Kirtland AFB, New Mexico, (1996).

Klein, M. V., T. E. Furtak, Optics, 2nd edition, John Wiley & Sons, New York, (1986).

Lillesand, T.M., R. W. Kiefer, Remote Sensing and Image Interpretation, 3rd edition, John Wiley & Sons, Inc., New York, (1994).

Melles Griot, "Optics Guide 5", Melles Griot Inc., Irvine, California, (1990).

Nee, S. F., "Polarization Characterization for Target Surfaces", SPIE Proceedings Vol 2469, (1995).

Nee, T., Nee, S. F., "Infrared Polarization Signatures for Targets", SPIE Proceedings Vol 2469, (1995).

Reitz, J. R., F. J. Milford, R. W. Christy, Foundations of Electromagnetic Theory, 4th edition, Addison-Wesley Publishing Company, New York, (1993).

Rogne, T. J., Smith, F. G., Rice, J. E., "Passive Target Detection using Polarized Components of Infrared Signatures", SPIE Proceedings Vol 1317, 242-251, (1990).

Rogne, T. J., K. W. Gleichman, J. R. Maxwell, "Mid-Wave Infrared Imaging Polarimeter: Instrument Development and Background Measurements", Environmental Research Institute of Michigan, Ann Arbor, Michigan, (1995).

Sturgeon, M. A., "Spectral and Polarimetric Analysis of Hyperspectral Data Collected by an Acousto-Optic Tunable Filter System", Master's Thesis, Naval Postgraduate School, Monterey, California, (1993).

Wilson, J., Hawkes, J. F. B., Optoelectronics - An Introduction, 2nd edition, Prentice Hall, New York, (1989).

Zissis, G. J., Sources of Radiation, Infrared Information Analysis Center Environmental Research Institute of Michigan, Ann Arbor, Michigan, (1993).

INITIAL DISTRIBUTION LIST

1. Defense Technical Information Center2
8725 John J. Kingman Road, Ste 0944
Ft. Belvoir, Virginia 22060-6218
2. Dudley Knox Library2
Naval Postgraduate School
Monterey, California 93943-5002
3. Commander, Naval Space Command1
ATTN: N112
5280 4th Street
Dahlgren, VA 22448-5300
4. Chairman, Code SP1
Space Systems Academic Group
Naval Postgraduate School
Monterey, California 93943-5002
5. David Cleary, Code PH/CL5
Department of Physics
Naval Postgraduate School
Monterey, California 93943-5002
6. Richard C. Olsen, Code PH/OS2
Department of Physics
Naval Postgraduate School
Monterey, California 93943-5002
7. CDR David S. Petri2
12737Avante Drive
Silverdale, Washington 98383